COO-3134-31

Lamont-Doherty Geological Observatory of Columbia University
Palisades, New York 10964

A COMPREHENSIVE STUDY OF THE SEISMOTECTONICS OF THE EASTERN ALEUTIAN ARC AND ASSOCIATED VOLCANIC SYSTEMS

Annual Progress Report

March 1, 1980 - February 28, 1981

By

K.H. Jacob, J.N. Davies, L. House, L.R. Sykes, M. Reyners, K. Coles, J. Mori

S. McNutt, J. Peterson, J. Hauptman, D. Johnson,

J. Beavan, and O. Perez

Prepared for the U.S. Department of Energy

Under Contract DE-AS02-76 ERO-3134

DISCLAIMER

TABLE OF CONTENTS

ABSTRACT

Refined hypocenter locations beneath the Shumagin Islands seismic network of the eastern Aleutian arc, Alaska, provide for the first time conclusive evidence for a double-sheeted dipping seismic (Benioff) zone in this arc. This refined seismicity structure was obtained in the arc section centered on the Shumagin seismic gap. A thorough review of three seismic gaps in the eastern Aleutian arc shows a high potential for great earthquakes within the next one to two decades in the Shumagin and Yakataga seismic gaps, and a less certain potential for a large or great earthquake in the possible Unalaska gap. A tilt reversal was geodetically observed to have occurred in 1978/79 in the forearc region of the Shumagin gap and could indicate the onset of a precursory strain relief episode prior to a great quake. A comparative study of the Pavlof volcano seismicity with that of other recently active volcanoes (i.e. Mt. St. Helens) indicates that island-arc (explosive-type) volcanoes respond to small ambient, periodic stress changes (i.e. tides). Stress drop measurements from earthquakes on the main thrust zone indicate high stress drops within the seismic gap regions of the Aleutian arc and low stress drops outside the gap region.

INTRODUCTION

This report describes completed research and related technical efforts carried out by Lamont-Doherty Geological Observatory during the first eight months, and outlines work in progress for the remaining four months of the contract period March 1, 1980 to February 28, 1981, of a

broad-based, comprehensive seismotectonic study of the eastern Aleutian arc and its volcanic systems. The region covered by this study is tectonically characterized by the occurrence of very large thrust earthquakes along a subduction zone and associated volcanic arc. The region studied requires attention from at least three points of view: (1) research on the basic tectonic and seismic processes at a convergent plate margin; (2) evaluation of energy resources in this tectonic environment which are potentially present as (a) hydrocarbon resources in the shelf regions, (b) geothermal resources associated with the volcanic arc, and (c) dispersed coal deposits; (3) evaluation of geologic hazards to the development of these resources. While this study focuses clearly on the first topic (basic seismologic and tectonic processes at a major segment of a convergent plate margin) the results described in this report directly affect the other two, more applied objectives (i.e. resources and hazards).

This project is aimed to provide both a broad overview of the seismicity and tectonics of a typical active subduction zone and associated volcanic arc as well as a detailed in-depth study of the microearthquake-activity and crustal deformation in this arc and of its associated volcanic systems. For the in-depth study we operate a regional telemetered network of some 30 seismic stations covering a 600 km long arc segment; this network includes a subarray of eleven stations densely spaced on and around Pavlof Volcano on the western portion of the Alaska Peninsula, for monitoring the seismicity associated with the magmatic processes in and beneath one of the most active volcanoes of the Aleutian arc. The Pavlof study is aimed towards basic volcanic research which will contribute to realistically evaluate the geothermal potential of some Aleutian volcanoes.

The cost for operating the eastern Aleutian seismic network is shared between this DOE-supported research program and a closely coordinated study under the Alaska Outer Continental Shelf Environmental Assessment Program (OCSEAP) administered by NOAA. OCSEAP urgently needs seismic hazards information for development of hydrocarbon resources on the vast Alaska shelf regions. The difficult logistic and climatic conditions and the vast expanse even of this small segment of the Aleutian arc (600 km long) require a level of effort both in manpower, logistic, and financial support which would by far exceed the fiscal limitations set for either of the two complimentary programs. It is therefore fortunate that both projects rely on the same seismological data base and hence can share the high cost for network maintenance and technical realization.

RESEARCH HIGHLIGHTS

Highlights in research and technical results during the past contract period include:

- Identification of the fine structure within the dipping seismic zone beneath the Shumagin Islands (including identification of a double-sheeted Benioff-zone from seismic network data).
- Quantization of the seismic potential in three seismic gaps in the Alaska- eastern Aleutian arc (Shumagin, Yakataga, Unalaska seismic gaps).
- An opportunity to compare results from our study of seismicity of Pavlof volcano with that of Mt. St. Helens; both studies have severe implications for magma transport in explosive-type volcanoes.

- Improvements in seismic field installations and their impact on digital data analysis.

Other supporting or related research efforts produced results on stress-drop associated with moderate-sized events in the eastern Aleutians and confirmation of an apparent reversal in polarity of crustal deformation in the Shumagin gap region that apparently occurred in 1978/79. The latter may be an indicator of the imminence of a great earthquake in the Shumagin seismic gap.

A major breakthrough was achieved [Reyners and Coles, 1980; and in preparation] by refining the structures associated with seismic activity beneath the Shumagin Islands. First a highly scrutinized set of seismic network hypocenter locations was used to show that at depths between about 60 and 120 km a double-sheeted dipping seismic (Benioff) zone exists. Second, Reyners and Coles obtained composite fault plane solutions from events within the two seismic bands and showed that they represent differing stress regimes. Thirdly, they used converted phases originating from the top of the subducting slab to constrain its exact depth and the velocity contrast across it. Only in Japan and New Zealand has it heretofore been possible to resolve such details in the seismicity of subducting slabs.

Probably one of the most powerful tools which recently has been developed for understanding the timing and occurrence of great subduction zone earthquakes is the concept of Seismic Gaps [Sykes, 1971; Kelleher, 1971; McCann et al., 1979]. We have completed a thorough survey of all historic and instrumental seismic data in the Alaska-eastern Aleutian arc regions and identified two well defined seismic gaps and a possible third gap. These results are now either published, in press, or submitted for

publication in a series of papers which concern, respectively, the entire Alaska-Aleutian arc [Sykes et al., 1980; Sykes et al., 1981], the Shumagin Gap [Davies et al., 1981], the Yakataga Gap [McCann et al., 1980; Perez and Jacob, 1980a, 1980b], and the possible Unalaska gap [House et al., 1980]. Furthermore the study of seismic gaps and of histories of great earthquakes strongly contributed to improve the understanding of recurrence times for great earthquakes along any major plate boundary as a function of rate and direction of plate motion, ratio of seismic to aseismic energy release, plate boundary geometry and variation in stress drops [Sykes and Quittmeyer, 1980, 1981]. The result of this study will be instrumental for reducing the uncertainty in the recurrence times of future great earthquakes.

The explosive eruptions of Mt. St. Helens volcano, Washington, provided a timely opportunity to apply recent results of McNutt [1979] from his study of the Aleutian volcano Pavlof to a generalization of processes associated with magma transport in explosive-type volcanoes. McNutt uses volcanic seismicity as an indicator of volcanic activity and finds that exterior stress variations (tidal forces) can enhance both extensional and contractional phases during eruptive activity, but at different times. This comparative volcano seismicity study is still in progress.

Several major improvements were achieved in the technical status of the eastern Aleutian seismic network operated by Lamont-Doherty. Event-detecting analog-tape recording systems were installed and are operative in Dutch Harbor (Unalaska Is.) and in Sand Point (Shumagin Is.). A digital recording system has been built for installation at Sand Point in December 1980. Satellite precision clocks were installed in all three

central recording sites (Dutch Harbor, Sand Point, Saint Paul) and synchronize the time bases at these three sites within 1/1000 sec. Six new strong motion recording sites were established in the Shumagin Islands with supplemental funding by the U.S. Geological Survey. These and other technical improvements particularly tuned towards digitally processing the network data will have a major impact on the speed of analysis and quality of research to be carried out in future years. Major impacts of these technical improvements concern time resolution in studying seismic delays caused by magma chambers beneath Pavlof volcano, accuracy of hypocenter locations, and seismic wave-form analysis for source, attenuation and strong-motion studies.

The following paragraphs provide research results and technical information in greater detail for each research topic.

RESEARCH RESULTS AND PROGRESS

Evaluation of Seismic Potential in Two Seismic Gaps Completed:

Shumagin Islands Gap. Using the new compilations of historic and instrumental data on seismicity of the entire Alaska Aleutian arc [Sykes et al., 1980; Sykes et al., 1981], Davies et al. [1981] have completed a thorough analysis of the Shumagin seismic gap. Their major results are:

The Shumagin seismic gap (Figure 1), a segment of the plate boundary along the eastern Aleutian arc, has not ruptured during a great earthquake since at least 1899-1903. Because at least 77 years have elapsed since the Shumagin Gap last ruptured in a great earthquake and repeat times for the 1939 rupture zone and part of the Shumagin Gap are estimated to be 50 to 90 years, a high probability exists for a great earthquake to occur within the

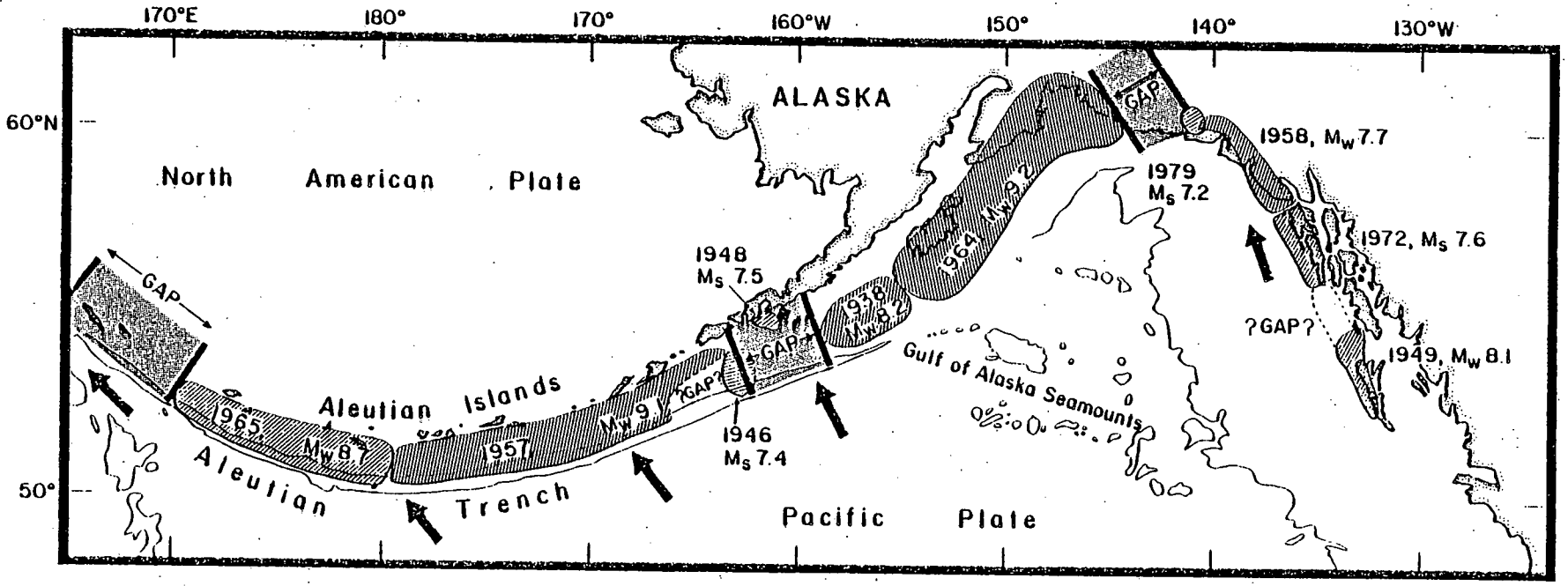

Figure 1. Aftershock areas of earthquakes of magnitude $\geq$ 7.4 in the Aleutians, southern Alaska and offshore British Columbia from 1938 to 1979, after Sykes (1971) and McCann et al. (1980). Heavy arrows denote motion of Pacific plate with respect to North American plate as calculated by Chase (1978) and Minster and Jordan (1978). Two thousand fathom contour is shown for Aleutian trench. M_S and M_W denote magnitude scales described by Kanamori (1977). Shumagin Gap is in center of figure.

Shumagin Gap during the next one to two decades. Reconsideration of the rupture zones of the Aleutian earthquakes of 1938, 1946 and 1948 suggests that those events did not break the interplate boundary beneath the Shumagin Islands. Thus, the Shumagin seismic gap extends from the western end of the 1938 rupture zone to the eastern end of that of 1946. These boundaries also coincide with transverse structural features. At least the eastern half of the Shumagin Gap broke in great earthquakes in 1788 and 1847 and possibly in 1898-1903 (Figure 2). The Shumagin Gap is probably not the result of aseismic slip; rather, plate motion is accommodated there seismically and episodically and can be expected to produce large earthquakes in the future. Although there is no definitive evidence of long-term precursors of a possible future earthquake, several observations suggest that the Shuamgin Gap is in an advanced stage of the earthquake cycle. Both teleseismic and local network data indicate a near absence of seismic activity ($M \geq 2$) above a depth of 30 km along the main-thrust zone within the gap; this is in strong contrast to adjacent portions of the arc where seismic activity is scattered across most of the main-thrust zone. Two earthquakes with high stress-drops (600-900 bars), which occurred at the base of the main-thrust zone, may indicate the accumulation of a considerable amount of strain energy within the gap. A possible seismic gap at the eastern end of the aftershock zone of the Aleutian earthquake of 1957 has been identified near Unalaska Island. An earthquake that nucleates in the Shumagin Gap could also rupture the possible Unalaska Gap to the west, the 1938 aftershock zone to the east, or both, with resultant magnitude up to $M_w = 9.0$. Alternatively, the Shumagin Gap alone, or in one of the above combinations could rupture in a series of very large earthquakes instead of a single great shock. Past Alaska-Aleutian earthquakes,

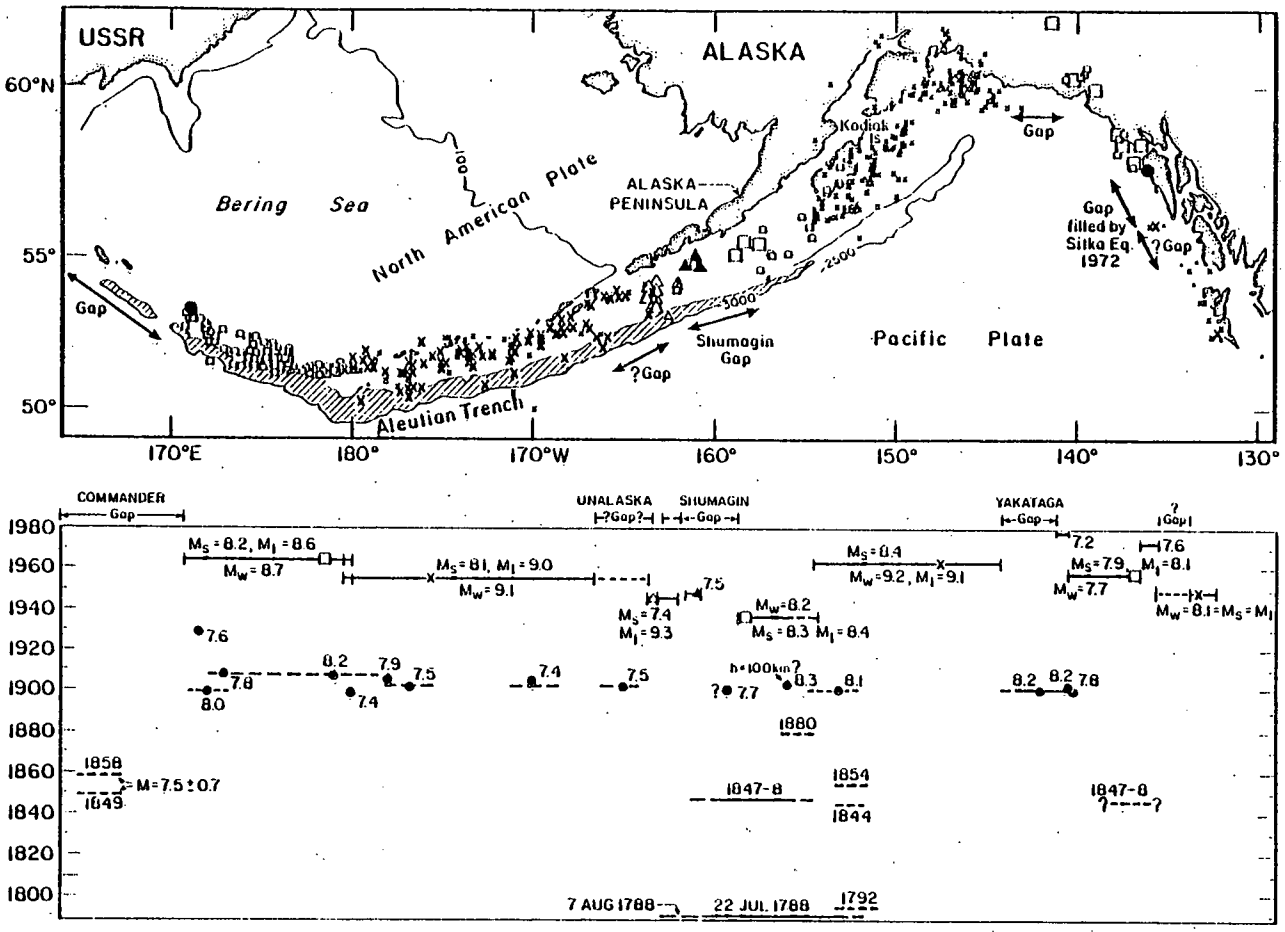

Figure 2. Above: Aftershocks of earthquakes of magnitude ≥ 7.4 from 1925-1971 along plate boundary in Aleutians, southern Alaska and offshore British Columbia, after Sykes (1971). Contours in fathoms. Various symbols denote individual aftershock sequences as follows: crosses, 1949, 1957 and 1964; squares, 1938, 1958 and 1965; open triangles, 1946; solid triangles, 1948; solid circles, 1929, 1972. Largest symbols denote most precise locations. Aftershock zone dimensions usually could not be determined before about 1925. Note that for the 1938 event two aftershocks indicated by open squares, appear to fall within the Shumagin Gap; see discussion in text. Below: Space-time diagram showing lengths of inferred rupture zones, magnitudes and locations of mainshocks for known events of M ≥ 7.4 from 1784 to 1980. Dashes denote uncertainties in size of rupture zones. Magnitudes pertain to surface wave scale, M_S unless otherwise indicated. M_W is ultra-long period magnitude of Kanamori (1977); M_t is tsunami magnitude of Abe (1979). Large shocks in 1929 and 1965 that involve normal faulting in trench are omitted. Absence of shocks before 1898 along several portions of plate boundary reflects lack of an historic record of earthquakes for those areas. Magnitudes after Richter (1958), Kanamori (1977), Kondorskaya and Shebalin (1977), Kanamori and Abe (1979) and Perez and Jacob (1980).

including those of 1788, 1938, 1946, 1957, 1964, and 1965, have generated very large tsunamis (Figure 3). Future large earthquakes in the Shumagin Islands region could generate wave heights of several tens of meters along shorelines near the rupture areas. The Shumagin Gap is one of two major gaps along the United States portion of the Alaska-Aleutian plate boundary and is one of the few areas in the United States where processes leading to a great earthquake are likely to be observed within a reasonable span of time.

Yakataga Seismic Gap. Macroseismic data for the great earthquakes of 4 and 10 September 1899 in the eastern Gulf of Alaska (Figure 2) indicate that much of the plate boundary between the 1958 and 1964 earthquakes ruptured at that time. The potential slip that may have been built up in the region from 1899 to the present is similar to the average slip associated with the 1899 events. Focal mechanism solutions nd geologic studies indicate that convergent plate motion in the region is accommodated in shallow thrust planes, as in the zone to the west that ruptured in the 1964 Alaska earthquake. A large portion of this thrust zone has been nearly quiescent for events as small as magnitude 4.0 for the last 15 years. This zone of near quiescence is surrounded by a ring of activity. The number of larger earthquakes in the ring appears to have increased significantly since the 1958 earthquake on the adjacent plate boundary. This doughnut-like pattern resembles in many ways the spatial-temporal patterns that preceded several great earthquakes. The spatial and temporal changes that we observed within the Yakataga gap, however, do not permit us to estimate precisely the time of occurrence of a future great shock that would rupture the gap. Intensified field studies are needed to identify effects that may be precursory to such an event. Never-

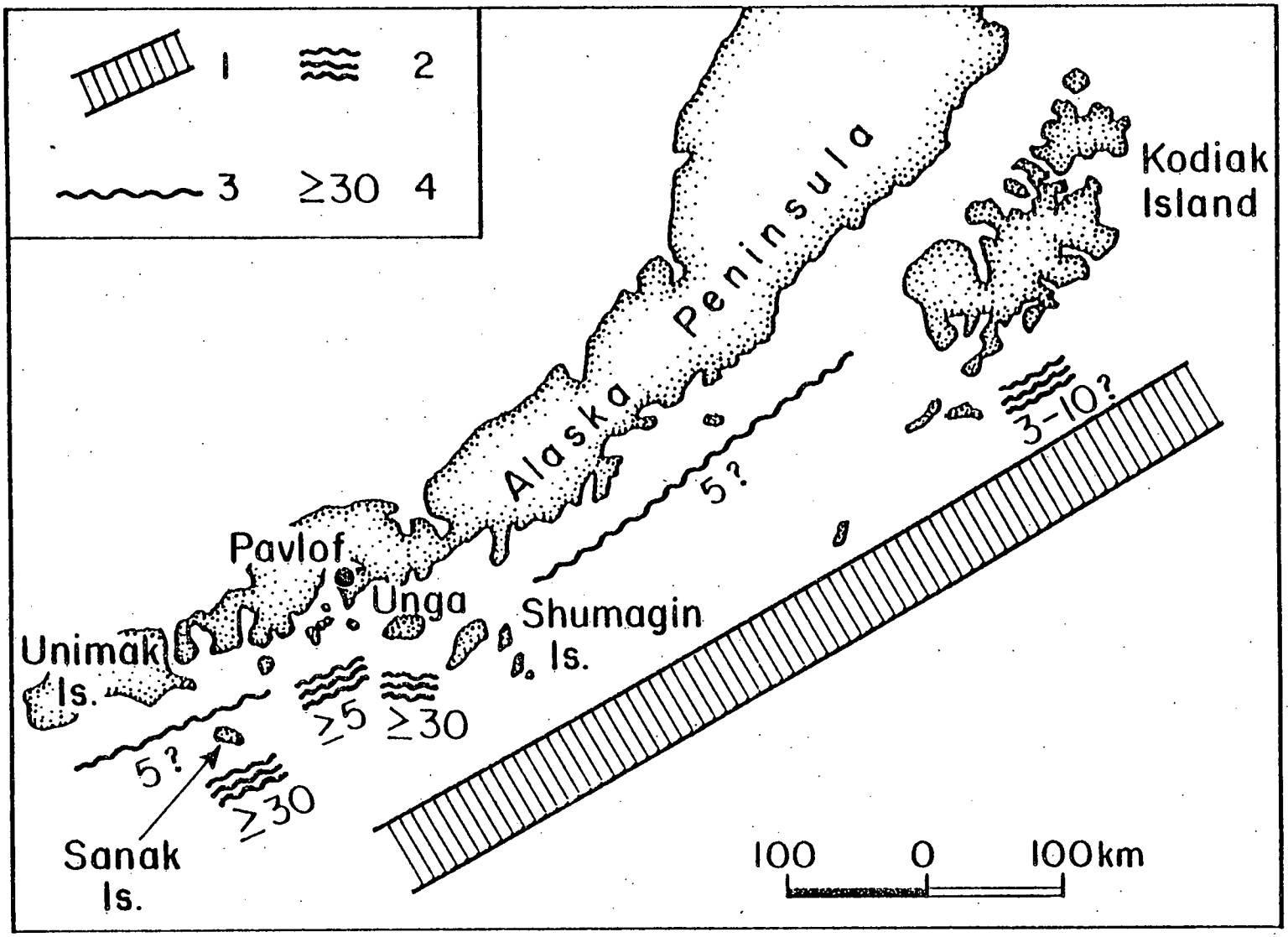

Figure 3. Diagram of earthquakes and tsunami of 1788, after Solov'iev (1968). 1 - hypothetical location of rupture zone; 2 = positive known places of appearance of tsunami, 3 - probable places of appearance of tsunami; 4 - approximate height of tsunami in meters.

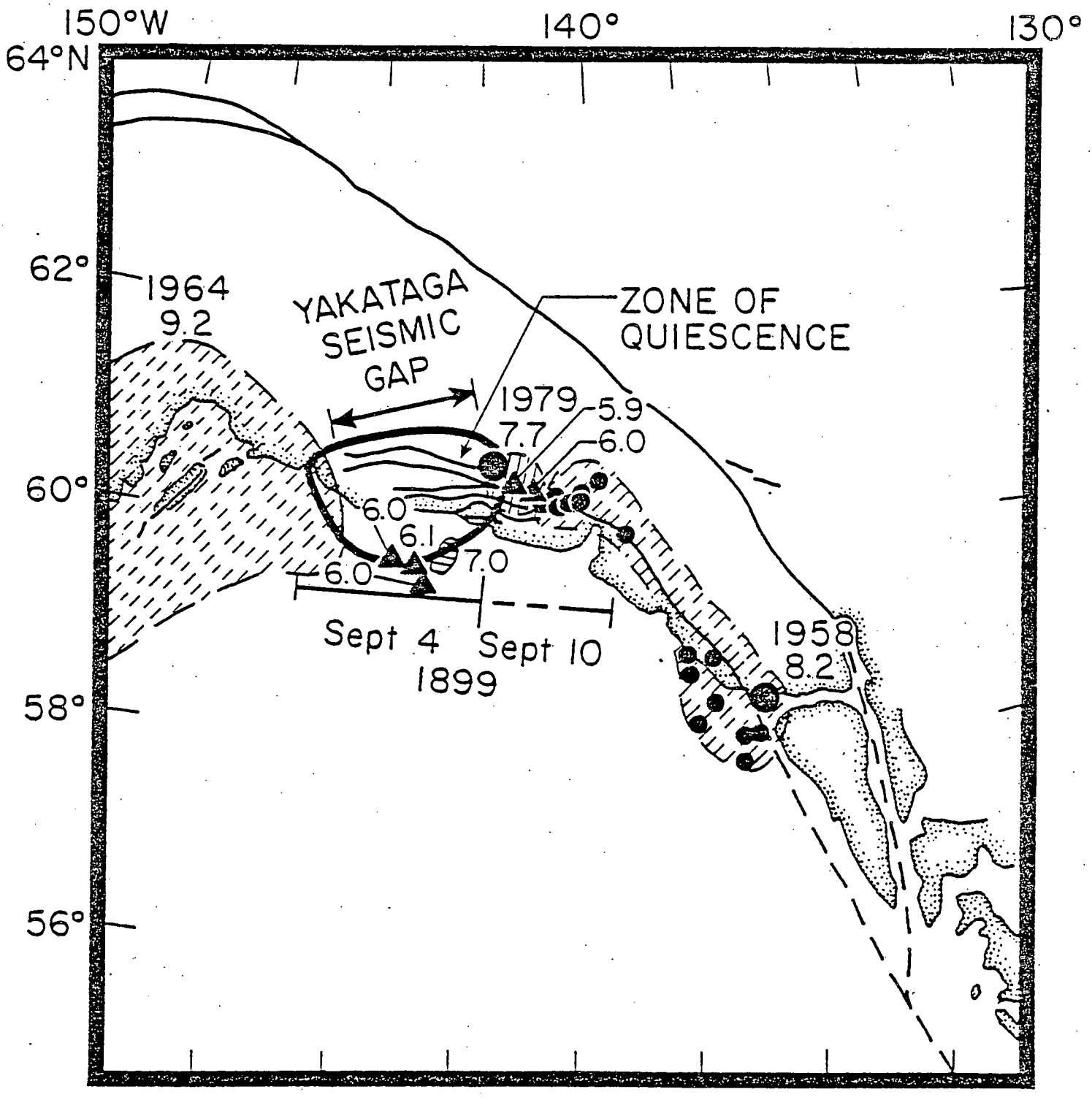

Figure 4. Earthquakes of magnitude 5.9 or larger near the Yakataga seismic gap from January 1958 to February 1979. Note that seven of these events are situated at the edges of the zone of near quiescence for small shocks (heavy solid line) shown in Figure 2. Large circles denote the epicenters of main shocks of large events in 1958 and 1979; small circles, aftershocks of the 1958 earthquake; triangles, shocks of magnitude 5.9 to 7.0. Faults are from King (1967). Inferred lengths of the rupture zones of two great earthquakes in 1899 are indicated. Hatching indicates the rupture zones of the 1958 and 1964 earthquakes. Numbers below dates are magnitudes.

theless, the observation that this region ruptured in a series of large shocks in 1899, the calculation of a repeat time of about 80 years, and the occurrence of a large earthquake in the area in 1979 suggest that the Yakataga gap is likely to be the site of a great earthquake within the next 10 to 20 years.

Identification of a Possible Seismic Gap Near Unalaska Island, Eastern Aleutians, Alaska

This study focuses on the easternmost (200 km long) portion of the 1200 km long aftershock zone of the great, M_w = 9.1, Andreanof-Fox Islands earthquake of 1957. Figure 2 illustrates the aftershock zone of this earthquake and its relation to several other great ($M \geq 7.8$) earthquakes that have broken portions of the Alaska-Aleutian plate margin in the past 100-200 years. By studying both seismicity and tsunami data, we conclude that the easternmost 200 km (the Unalaska segment) of the 1957 aftershock zone underwent deformation in a manner quite different from the remaining 1000 km long zone and may not have ruptured in 1957. If it did not rupture in 1957, it could have significant impact on the evaluation of seismic and tsunami hazards in the eastern Aleutians.

Seismicity Data. Figure 5 is a map view of the eastern Aleutians and illustrates the location of the 1957 mainshock (shaded) and aftershocks that occurred within one year after the main shock. The distribution of aftershocks is fairly heterogeneous, yet, between about 180°W and 166°W, aftershocks occur over a zone some 80 km wide, measured normal to the strike of the arc. In contrast, those aftershocks within the easternmost 200 km of the 1957 aftershock zone align only at the arcward (northern)

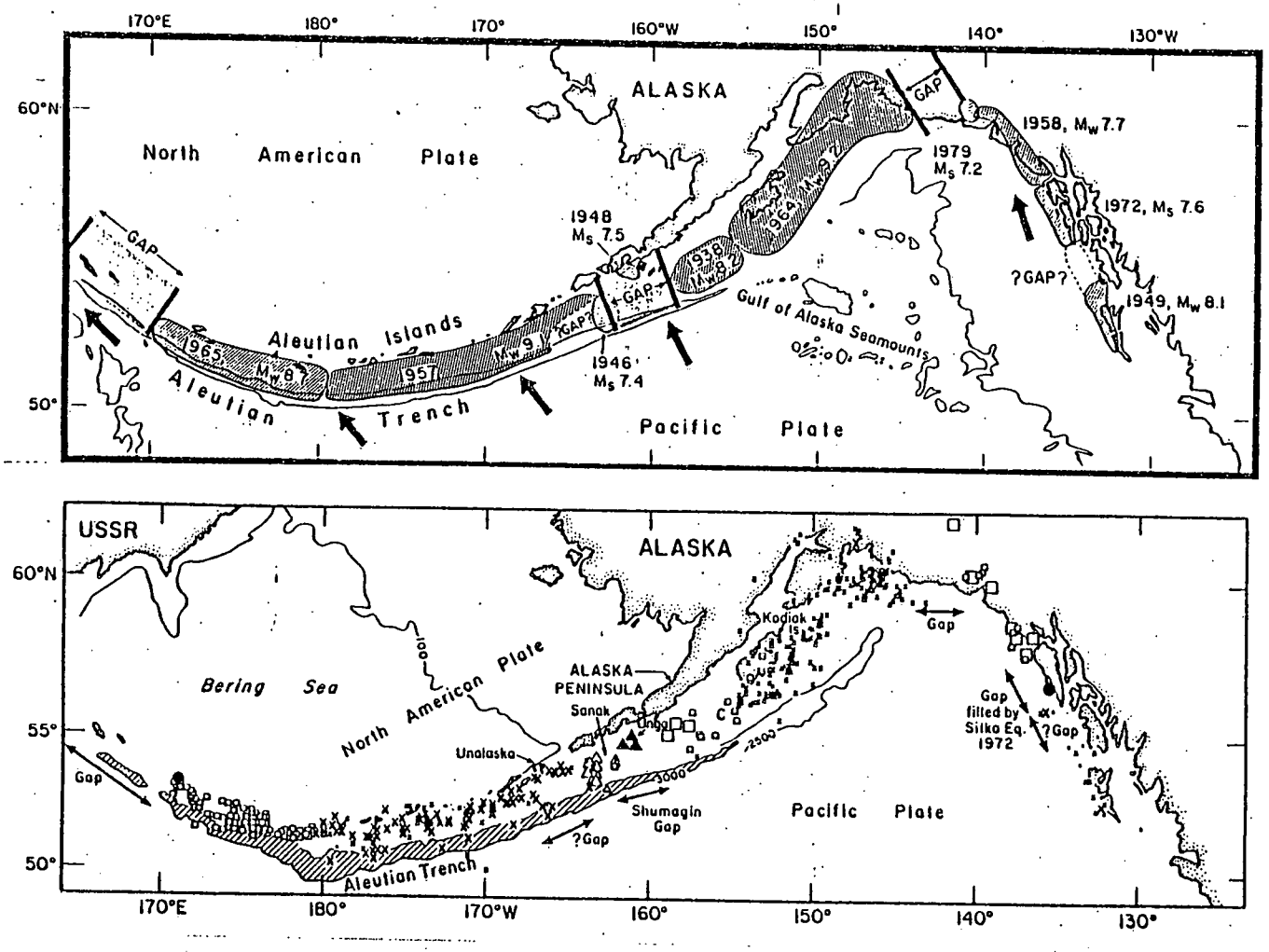

Figure 5. Top: Location map and identification of aftershock zones of major earthquakes and previously identified seismic gaps in Alaska and the Aleutians. The possible Unalaska Gap is the area labelled as a queried gap near 165°W. Note the proximity of the 1946 tsunamigenic earthquake to the possible Unalaska Gap, and also that the Shumagin Gap nearly abuts the eastern edge of the possible Unalaska Gap. Arrows indicate direction of relative convergence. (After Davies et al., 1981). Bottom: Map of relocated aftershocks of recent major earthquakes in Alaska and the Aleutians. Only those aftershocks of the 1957 earthquake that occurred in March of 1957 are included; these are plotted as large X's. Note how far trenchward the aftershocks extend between 180°W and 166°W as compared to the very narrow band between 166°W and 163°W. Also note that 3 aftershocks plot within the aftershock zone of the 1946 earthquake, which is identified by triangles (see text for discussion of these events). Bathymetry is in fathoms (1 fathom = 1.83 m). (After Sykes, 1971).

edge of the aftershock zone. We term this easternmost 200 km long portion the Unalaska segment and the remaining 1000 km zone, the main segment. Note also (Figure 5) the lack of aftershocks beneath the portion of the trench seaward of the Unalaska segment. From the time history of seismicity that occurred beneath the trench between about 163°W and 180°W, House et al [1981] conclude that such activity (Figure 5) represents events that were stimulated by the 1957 main shock. The lack of activity beneath the trench seaward of the Unalaska segment suggests that the Unalaska segment may not have broken in 1957.

The distribution of seismic activity prior to the 1957 main shock (Figure 6) reinforces the initial impressions obtained from the aftershock distribution. Two notable clusters of activity occurred in the 11 years prior to the 1957 main shock. The location of one, near 180°W, coincides with the western extent of aftershock activity. A more intense cluster occurred near the eastern end of the main segment of the 1957 aftershock zone (about 168°W). In a simple interpretation, these clusters may have resulted from precursory fracture or slip along the two ends of the impending rupture zone.

Tsunami Data. The good agreement between the aftershock areas and the tsunami source areas of major underthrust-type earthquakes [Hatori, 1970; Nishenko and McCann, 1979] provides another way of constraining the rupture area of the 1957 earthquake. Ordinarily, tsunami wavefront diagrams are drawn that represent tsunami travel times along various paths. Tsunami speeds are well represented by the simple formula $S = (gh)^{1/2}$, where g is the acceleration due to gravity (9.8 m/s^2) and h is the depth, in meters. From the observed tsunami travel times to tide gauges located at various azimuths from the earthquake, the tsunami source

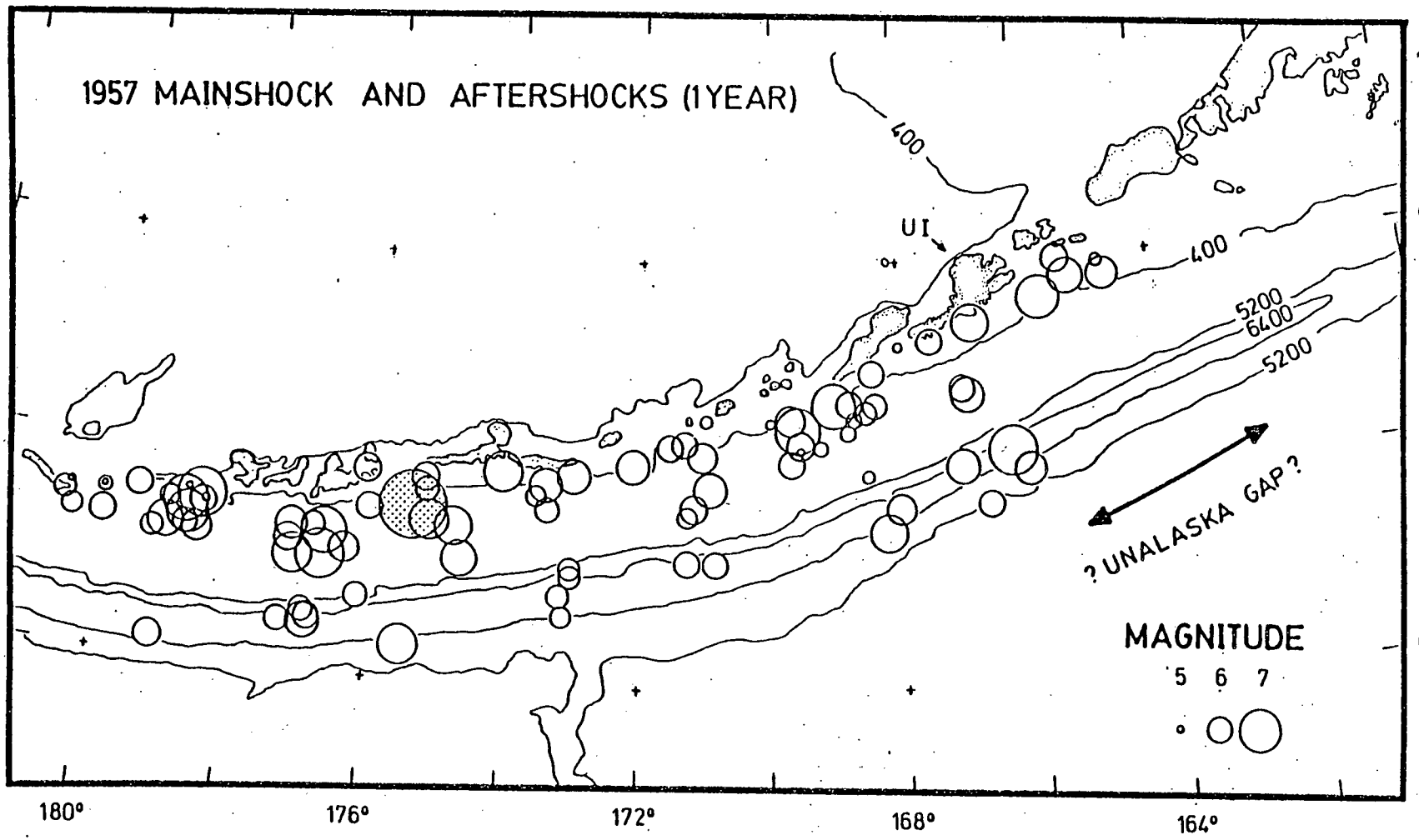

Figure 6. Detailed plot of the 1957 main shock and aftershocks over a period of 1 year. Aftershocks of March 1957 relocated by Sykes (1971) are supplemented by aftershocks located by the International Seismological Summary and the U.S. Coast and Geodetic Survey. Size of symbols is scaled to magnitude; only events assigned a magnitude of 5 or larger are plotted. The 1957 main shock is shaded and is plotted with a symbol size appropriate for its surface wave magnitude (M_S) of 8.2, rather than its M_W of 9.1. Earthquakes at depths shallower than 80 km are included although none occurred that were deeper than 60 km. UI indicates the location of Unalaska Island. Bathymetry is in meters.

area can be located. Using this approach, and the travel times of the 1957 tsunami to tide gauges on the west coast of North and South America, widely scattered estimates are obtained of the eastern extent of the 1957 tsunami source area [L.R. Sykes, unpublished data, 1979]. These scattered estimates make it impossible to distinguish whether the source area of the 1957 tsunami included only the main segment of the aftershock zone or whether it extended eastward and included the Unalaska segment.

To obtain a more precise location of the eastern extent of the tsunami source area of the 1957 earthquake we located it relative to that of another nearby earthquake. This method minimizes the effect of errors in the calculated travel times, since the only travel times that need to be calculated are those for the difference in the travel path between the reference event and the 1957 source area.

An earthquake located nearby that occurred in 1946 generated a large tsunami [Green, 1946; Shepard et al., 1950; Sykes, 1971; Kanamori, 1972; Fukao, 1979]. Davies et al. [1981] find that the aftershock and tsunami generating areas of the 1946 shock are nearly identical. Thus, it provides a good reference from which to locate the source of the 1957 tsunami. A total of six tide gauges recorded the tsunamis of both the 1946 and the 1957 earthquakes. From the differential travel times to these six tide gauges, we obtained five estimates of the eastern extent of the 1957 tsunami source area (locations from two of the tide gauges coincide). Figure 7 shows these estimates and their relation to the distribution of foreshock and aftershock activity.

We conclude that in 1957, the Unalaska segment must have deformed in a manner very different from that of the main segment of the 1957 aftershock zone. If the Unalaska segment ruptured in 1957 it must have done so in one

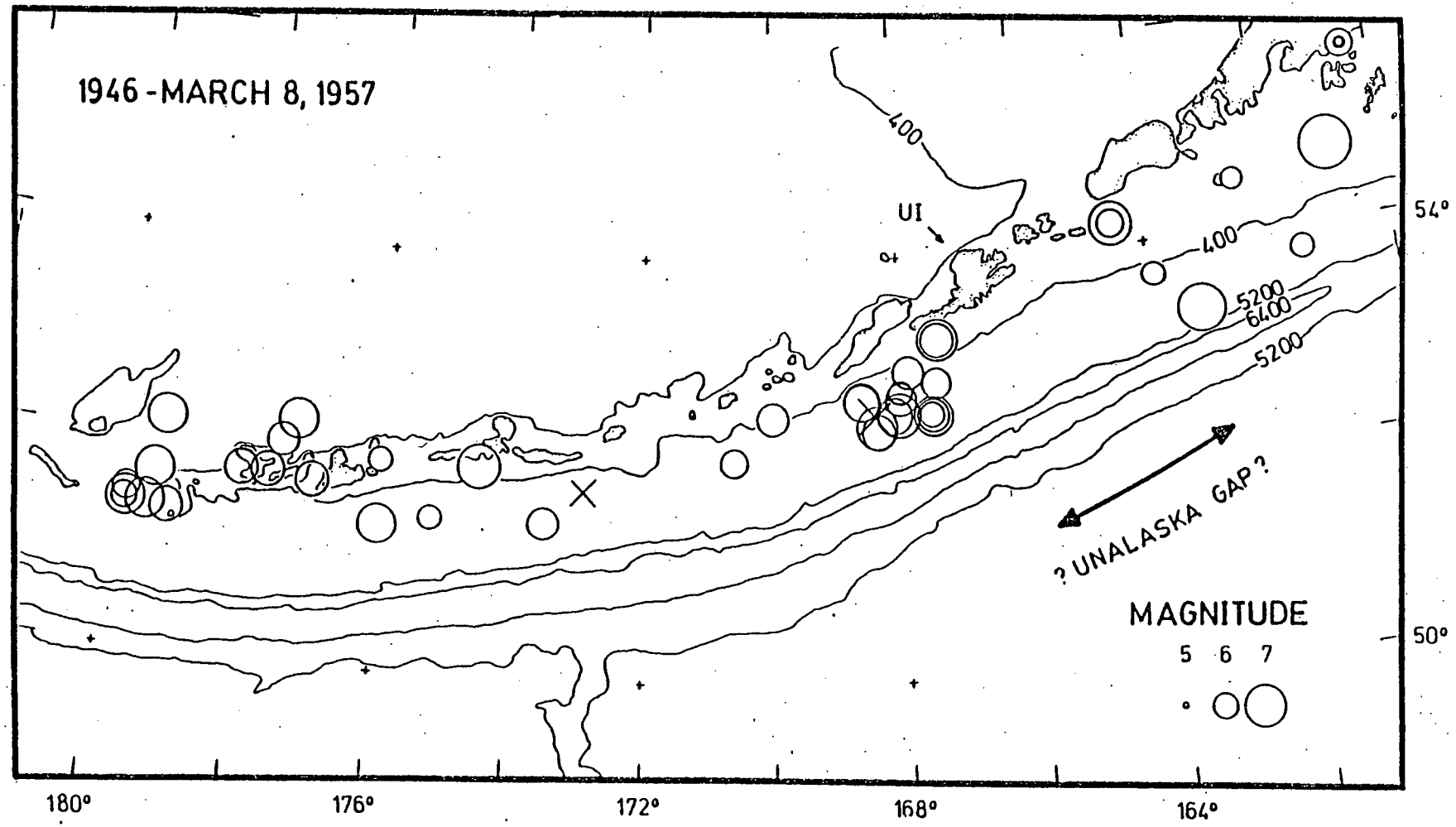

Figure 7. Plot similar to Figure 2, but of earthquakes from 1946 to just before the 1957 main shock. Earthquakes at depths shallower than 60 km are plotted as circles; those at depths of 60 to 80 km as X's. Note the clustering of epicenters near 180°W and near 168°W. Note also the location of the 1946 tsunamigenic earthquake, immediately to the left of the 5200 meter label.

of two ways. It may have ruptured as a normal rupture that was delayed sufficiently relative to the main earthquake rupture that its seismic and tsunami effects were indistinguishable from the coda of the main rupture. Alternatively, and more plausibly, the Unalaska segment could have ruptured in an event that was so slow that it took 100's of seconds. This type of rupture would be an inefficient source of a tsunami, and might be smooth enough not to generate aftershocks. Kanamori and Stewart [1979] term such an event a slow earthquake.

It is also possible, however, that the Unalaska segment did not rupture in 1957. If it did not, it could pose significant seismic and tsunami hazard to the eastern Aleutians. Although historic information does not indicate that the possible Unalaska gap has generated a great earthquake in the past, nearby portions of the Alaska-Aleutian plate margin definitely have [Davies et al., 1981; Sykes et al., 1981]. It would seem unwise, therefore, to consider the possible Unalaska Gap incapable of producing a great earthquake. Such an earthquake, if it were to rupture the entire area of the possible Unalaska Gap, could be as large as magnitude (M_w) 8.

Fine Structure of the Dipping Seismic Zone in the Shumagin Islands

An abiding problem in the analysis of microearthquake data from the Shumagin array is the rather incomplete knowledge we have of local crustal structure. No deep seismic sounding experiments have been undertaken in the area, and the crustal structure model routinely used for hypocenter determination is a synthesis of models determined by Matumoto and Page [1968] for the Cook Inlet area of Alaska, and Rowlett and Jacob [personal

communication, 1974] for the central and eastern Aleutian Islands. The horizontally-layered crustal model used is clearly but a first approximation, given the rather large variations in structure one might expect at a converging plate boundary. In order to obtain a sample of hypocenters relatively free of model errors, hypocenters not critically dependent on the adopted velocity model have been grouped together. In pratice, this has been achieved by requiring that the epicentral distance to the nearest station used in a hypocenter determination is less than or equal to twice the hypocentral depth. Such a procedure ensures good hypocentral depth control, as arrivals to the closet stations are interpreted as direct arrivals, the travel times of which are less prone to errors (due to an inadequate crustal structure model) than critically refracted arrivals, which may arrive first if the ratio of epicentral distance to hypocentral depth is large.

A depth section of well-determined hypocenters satisfying the above condition and occurring during the one and a half year period from July 1978 to December 1979 is shown in Figure 8. The section is oriented at N30°W, perpendicular to the strike of the arc; it has a width of 400 km and is centered on the Shumagin array. A N30°W orientation of the section gives the best definition of the dipping seismic zone. This definition is noticeably degraded if the section is rotated by as little a 2° in either direction. The dipping seismic zone shown in Figure 8 appears double-planed. The upper plane dips at 32° from 45 to 100 km depth, where it exhibits a knee-like bend below the volcanic front. The lower plane begins at about 65 km depth, where it is separated from the upper plane by some 25 km, and converges with the upper plane at about 125 km depth. This lower plane appears to be real, and not related to lateral segmentation of

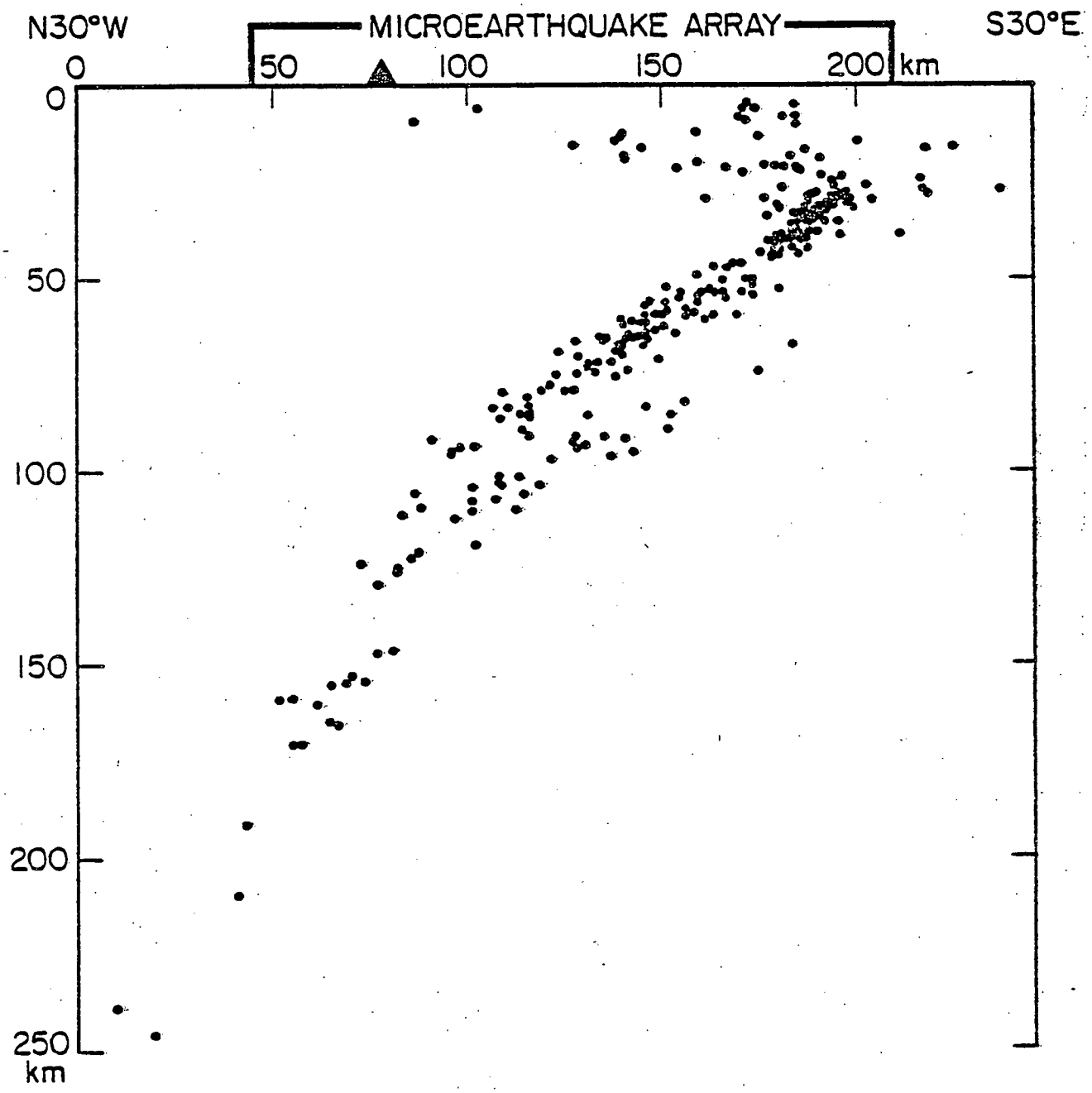

Figure 8. Depth section of well-determined hypocenters for the period July 1978 to December 1979. The section has a width of 400 km and is centered on the Shumagin Islands microearthquake array.

the subducted plate, since the microearthquakes comprising it are evenly spread along the strike of the arc. This is illustrated in Figure 9, which shows the lower plane hypocenters in map view. Indeed, the clear separation of the two planes of the dipping seismic zone evident in the 400 km-wide section shown in Figure 8 attests to the uniformity of the subducted Pacific plate along the strike of the arc in the region of the Shumagin array.

Double-planed seismic zones have recently been found in other areas of subduction, including the Kurile Islands [Veith, 1974], the Central Aleutian Islands [Engdahl and Scholz, 1977] and northeastern Japan [Hasegawa et al., 1978a,b]. Various explanations have been proposed for such zones, including elastic unbending of the subducted slab [Engdahl and Scholz, 1977], phase changes in the slab [Veith, 1974] and sagging of the slab under its own weight [Sleep, 1979]. Composite fault-plane solutions of the microearthquakes comprising the two planes of the seismic zone in the Shumagin Islands will provide constraints on the mechanism producing the double zone, and determination of such fault-plane solutions is currently underway.

A feature of the depth section shown in Figure 8 is the concentrated microearthquake activity in the 25-45 km depth range. The dip of this zone of activity is approximately 41°, some 9° steeper than that of the upper plane of the double-planed portion of the dipping seismic zone, lending credence to speculation that the double-planed portion of the zone represents elastic unbending of the subducted plate. A composite fault-plane solution indicates that the 25-45 km deep activity represents thrust faulting. As can be seen in Figure 10, the P axis of this composite fault-plane solution is near-horizontal, and its azimuth (330°) is very similar

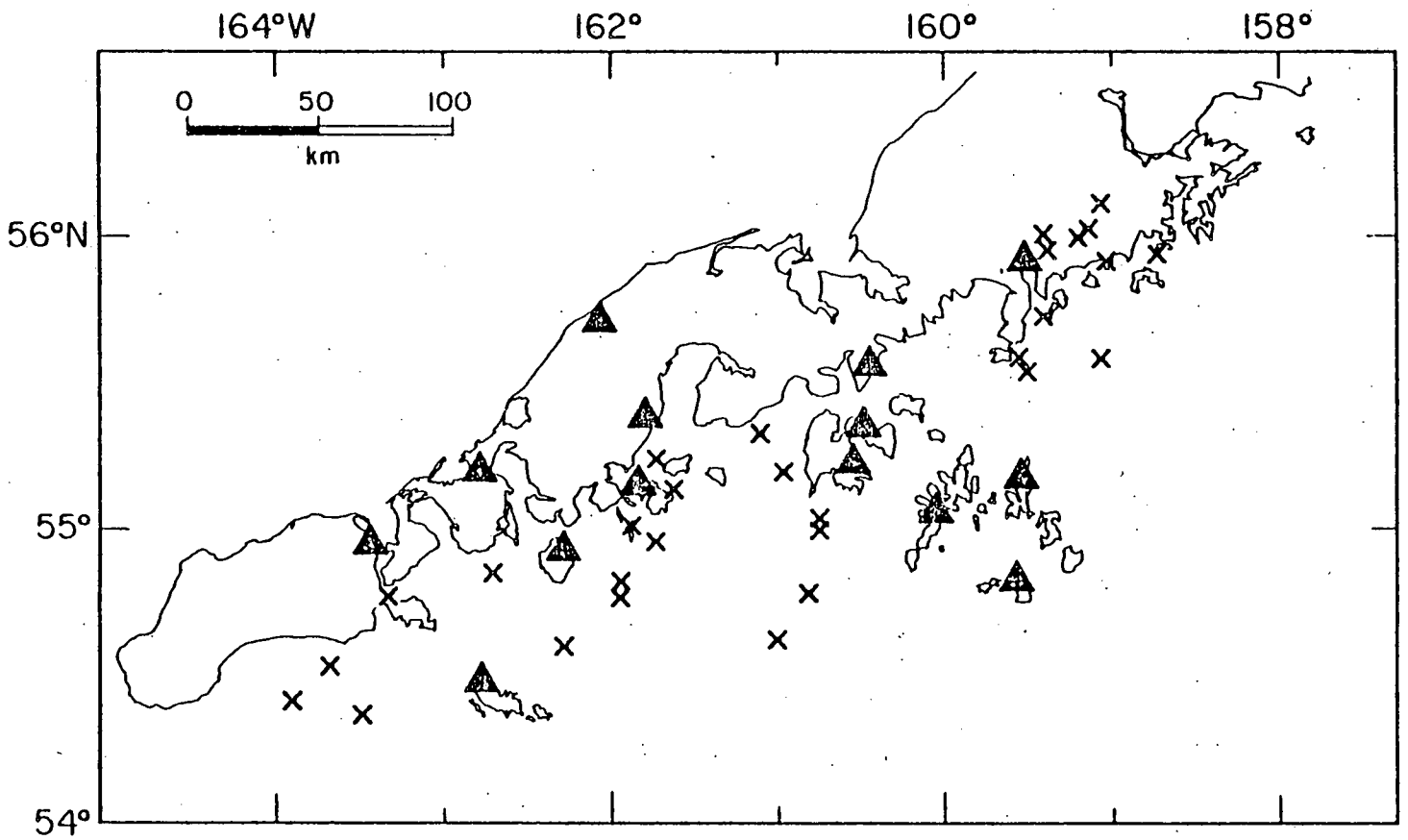

Figure 9. A map view of the hypocenters (crosses) comprising the lower plane of the double seismic zone evident in Figure 8. Solid triangles show seismic network stations.

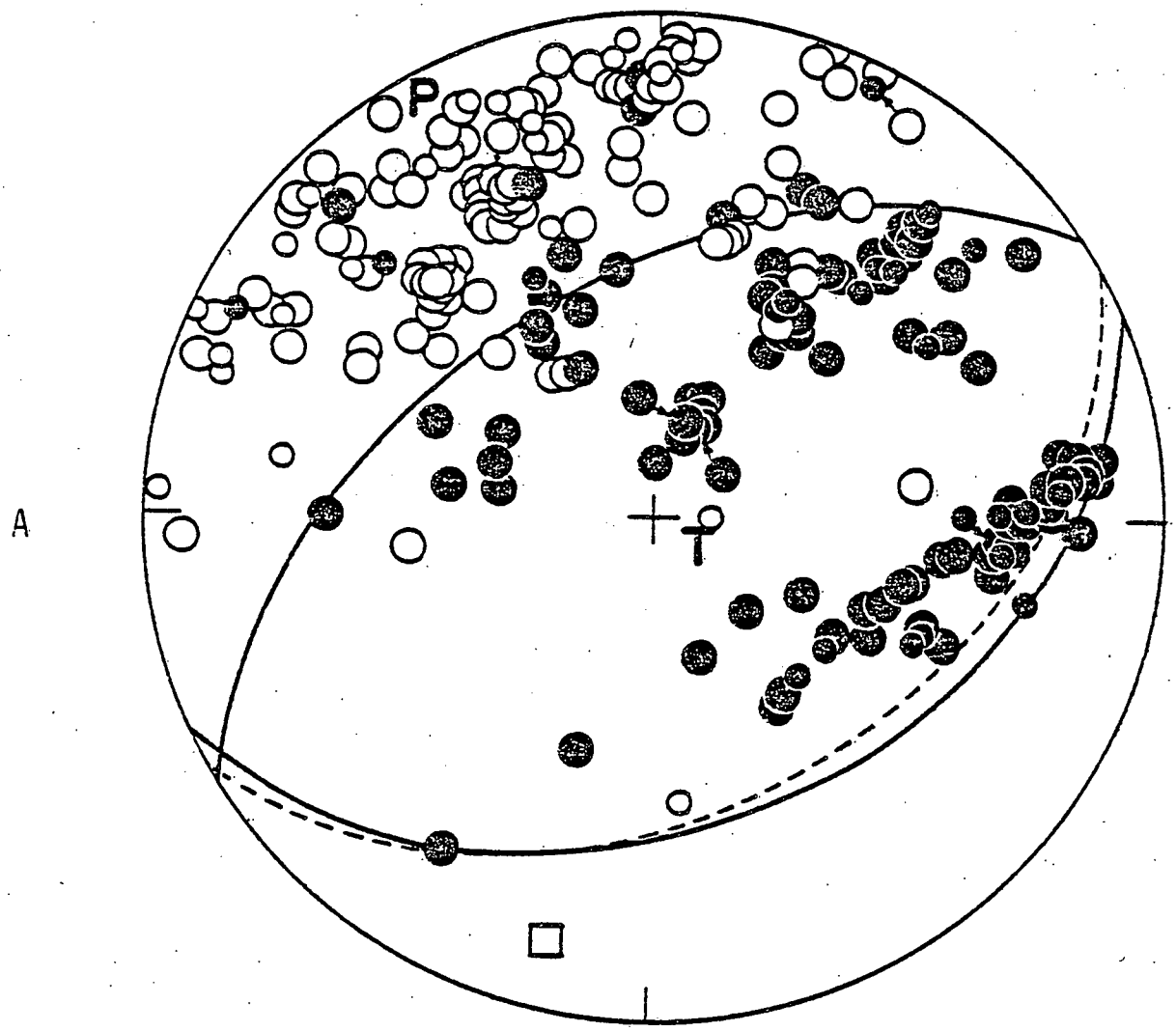

Figure 10. Upper-hemisphere, equal-area stereograms of first-motion directions for two groups of microearthquakes: (A) those comprising the dipping zone of concentrated activity in the 25-45 km depth range and (B)* those in the overlying plate landward of the group A events. Solid circles represent compressional arrivals; open, dilatational. P and T denote the axes of compression and tension, respectively. The dashed plane in fault-plane solution A shows the orientation of the dipping zone defined by the microearthquakes comprising the solution.

*(B) shown on next page.

B

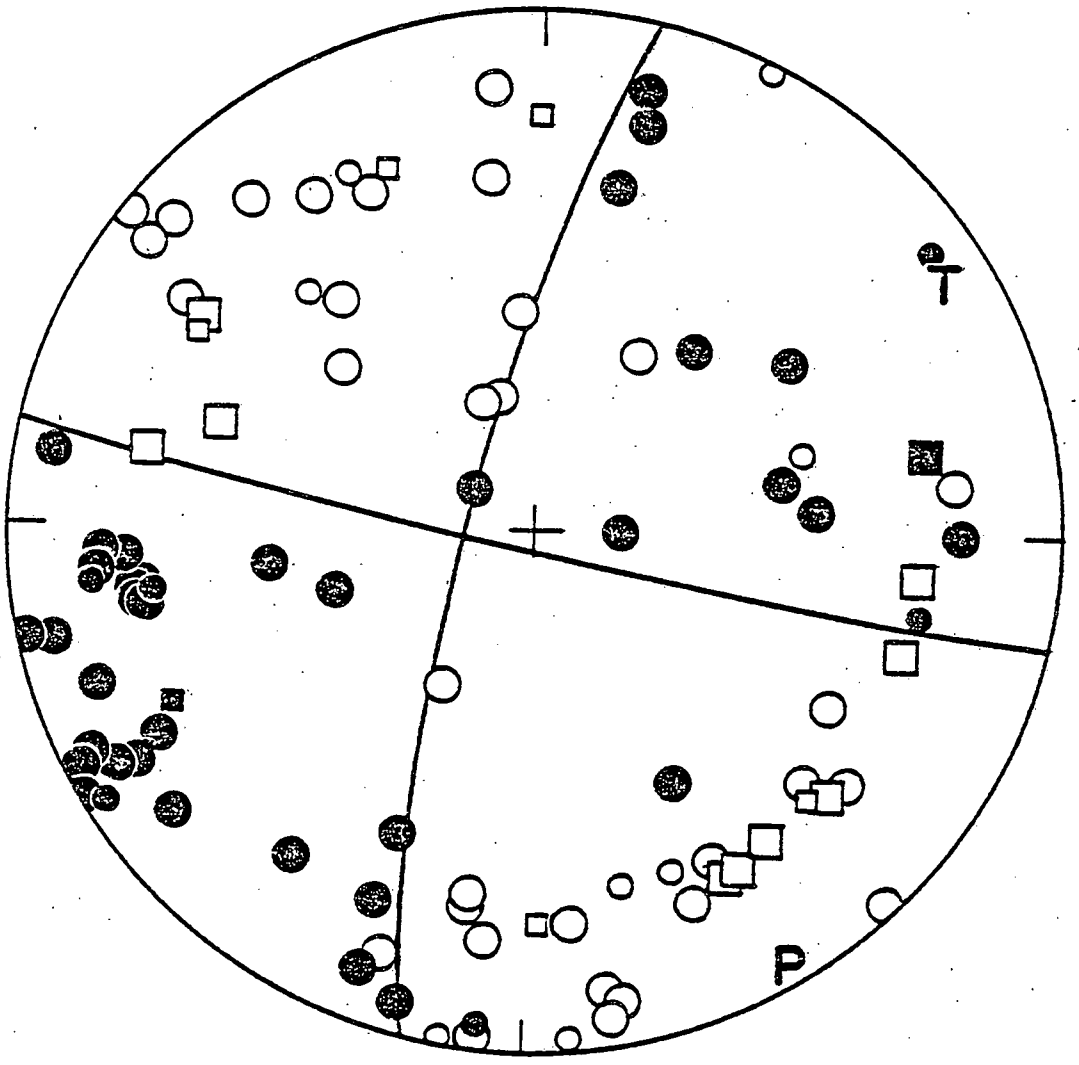

Figure 10 continued

to the azimuth of plate convergence predicted by the RM2 model of Minster and Jordan [1978] for the region of the Shumagin array (329°). In addition, one nodal plane of the solution is subparallel to the dipping zone defined by the 25-45 km deep activity. Landward of this activity, microearthquakes in the overlying North American plate show a strike-slip mechanism (see Figure 10), with the P-axis again near-horizontal and oriented in the direction of plate convergence. This result is consistent with the interpretation that the plate interface in the region of the Shumagin Islands is currently locked, with stresses due to plate convergence being transmitted to the overlying plate.

Pavlof/Mt. St. Helens Seismicity

During the past year we made progress in our studies of the seismic behavior of active volcanoes in the following fields: 1) Several additional months worth of Pavlof seismicity data (helicorder records) have been reduced; 2) the earth tide study has been completed and is being prepared for publication; 3) frequency analyses of some volcano seismic signals has been carried out; 4) tapes from our new event-detecting analog recording system have been played back and digitized for the magma chamber study; 5) to test Pavlof volcano results for their compatibility with other subduction-zone-related volcanoes we started a comparative study; for this purpose we initiated the following steps: (a) an investigation of short-term patterns of seismicity at Fuego and Pacaya Volcanoes (Guatemala), (b) preliminary b-values for the Mt. St. Helens earthquake sequence have been calculated. These areas will be described in detail in the following paragraphs.

As the recent eruptive activity of Mt. St. Helens has shown, subduction-zone related volcanoes can be quite unpredictable in their habits. Basic volcanic processes are only poorly understood, so an assessment of geothermal potential and volcanic hazards must of necessity be cautious until a data-based assessment can be established. We have expanded the scope of our volcano studies during the past year to include both Fuego and Pacaya (Guatemala) and Mt. St. Helens (Washington); the former in cooperation with David Harlow of the USGS and the latter in cooperation with the University of Washington Geophysics program. Our studies of Pavlof volcano will strongly benefit from such comparative studies of these other volcanoes. We have continued to investigate and quantify details of eruption processes and cycles using seismic information. This integrated, broad-based approach will best allow us to understand the basic physical processes in explosive volcanoes in general and of Pavlof's geothermal potential in particular.

A. Volcanic Seismicity Plots Based on Helicorder Records. Figure 11 shows a map of Pavlof volcano and vicinity with station locations. Records from the PVV station are nearly continuous from October 1973 to the present. These data were collected in cooperation with Juergen Kienle of the University of Alaska. At Lamont-Doherty we have made a summary of the number of volcanic earthquakes per day for the first seven month's of the station's operation (15 October 1973 - 15 April 1974), for the period 1 September 1974 - 30 April 1975, and for the month of September 1975. We are continuing this count up to the present time.

Histograms showing the number of events of four different types occurring during each 2 hour interval are also being routinely prepared for Pavlof Volcano. To date, helicorder records for the time period

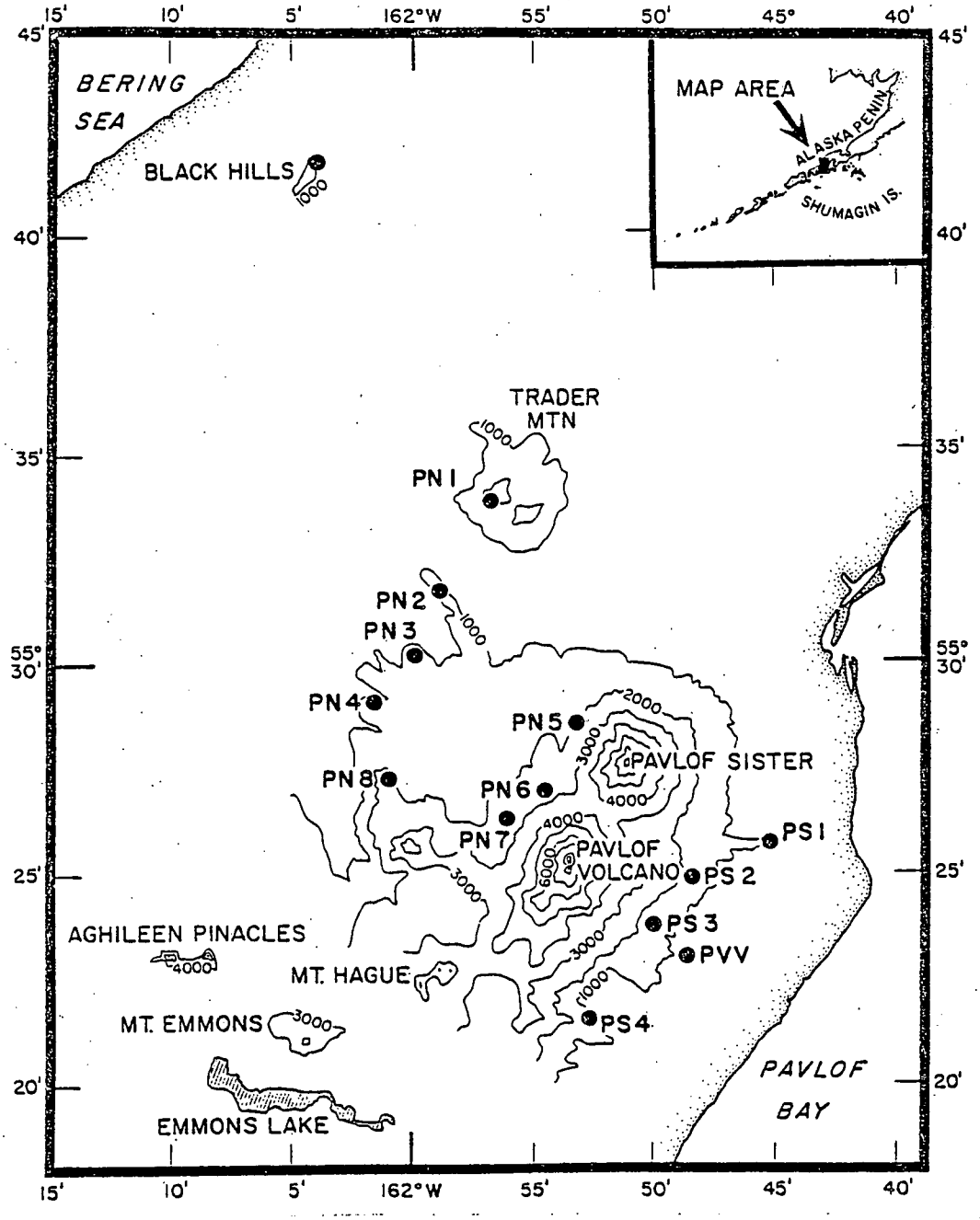

Figure 11. Location map showing seismometer stations around Pavlof Volcano. PVV and BLH are part of the Shumagin Islands Regional Network. PN1-8 and PS1-4 are stations of the Pavlof Local Network. PN1 and PN5 were removed during the summer 1980 field season.

1 September 1974 through 30 April 1975 and September 1975 have been systematically reduced. Number and size of b-type volcanic earthquakes, occurrence of air shocks, incidence and duration of harmonic tremor, and occurrence of high-frequency tremor have been catalogued for each 2 hour interval for the entire period. Figure 12 shows a sample of the data.

B. Earth Tide Study. The main results of the earth tide study are given in the abstract (Appendix 2) of a talk given at the Fall 1979 PNAGU Meeting. Figure 12 shows a portion of the data for which a correlation between earthquakes and tides is observed. Additionally, Figure 13 shows a schematic diagram illustrating our interpretation of the data. This work is presently being prepared for publication.

C. Frequency Analysis of Harmonic Tremor from Pavlof Volcano. Harmonic tremor signals from Pavlof volcano are observed on seismic records of eruptions. Signals resembling harmonic tremor are also observed on seismograms from stations near Tarbela dam and reservoir in Pakistan. Frequency analyses have been performed on both the Pavlof and Tarbela signals because we suspect a similar physical excitation process, i.e. intermittent high-velocity flow in a conduit. Two methods were used: Discrete Fast Fourier Transform and Burg maximum entropy. The Tarbela dam signals are shown to be organ pipe resonances in the outflow tunnels, with both even and odd harmonics present (i.e. $\lambda = 1/5\,\ell$, $1/2\,\ell$, $3/4\,\ell$, ℓ , $5/4\,\ell$, etc.). The observed spectra (Figure 14) change with location around the reservoir and with the size of the outflow opening, which is gate controlled.

We infer that the Pavlof harmonic tremor signals are also organ pipe resonances, presumably of a magma-filled conduit. The spectra (Figure 14) exhibit well-recorded higher frequencies, representing overtones such as

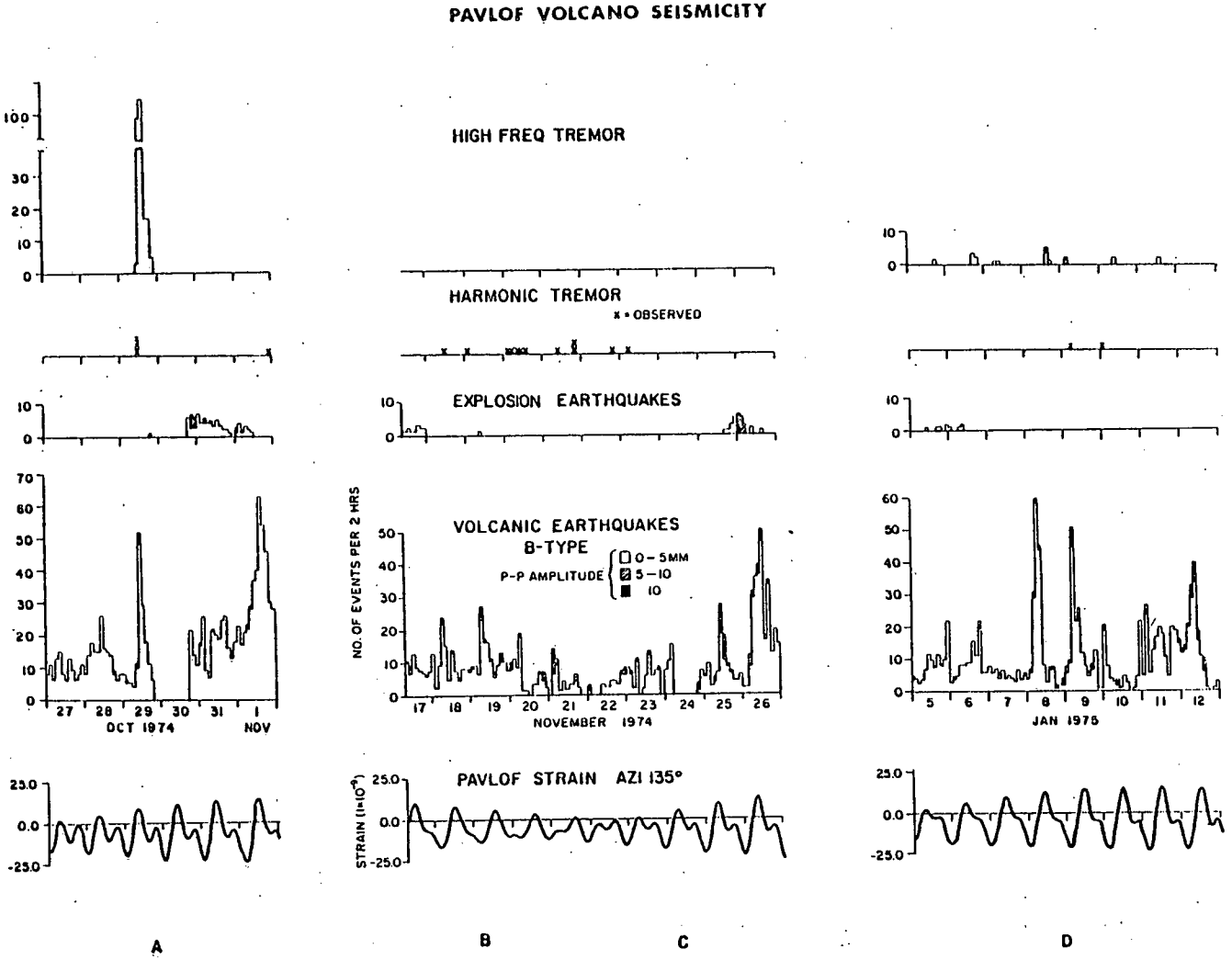

Figure 12. Comparison of different types of Pavlof volcano seismicity with horizontal tidal strain across the Aleutian arc. Note in particular the relation between the traces for the number of volcanic B-type earthquakes and the solid earth tidal strain in azimuth 135°. A and C label the beginning of eruptions, while B and D label the ends of eruptions. Note that during A and C peaks in the number of earthquakes just follow positive peaks in strain, while during B and D they just follow negative peaks in strain. It appears possible to interpret these data in terms of inflation and deflation, respectively, of the volcano prior to and following an eruption. Note that in this particular case ocean-load stresses were not accounted for and only astronomical solid-earth tides were computed.

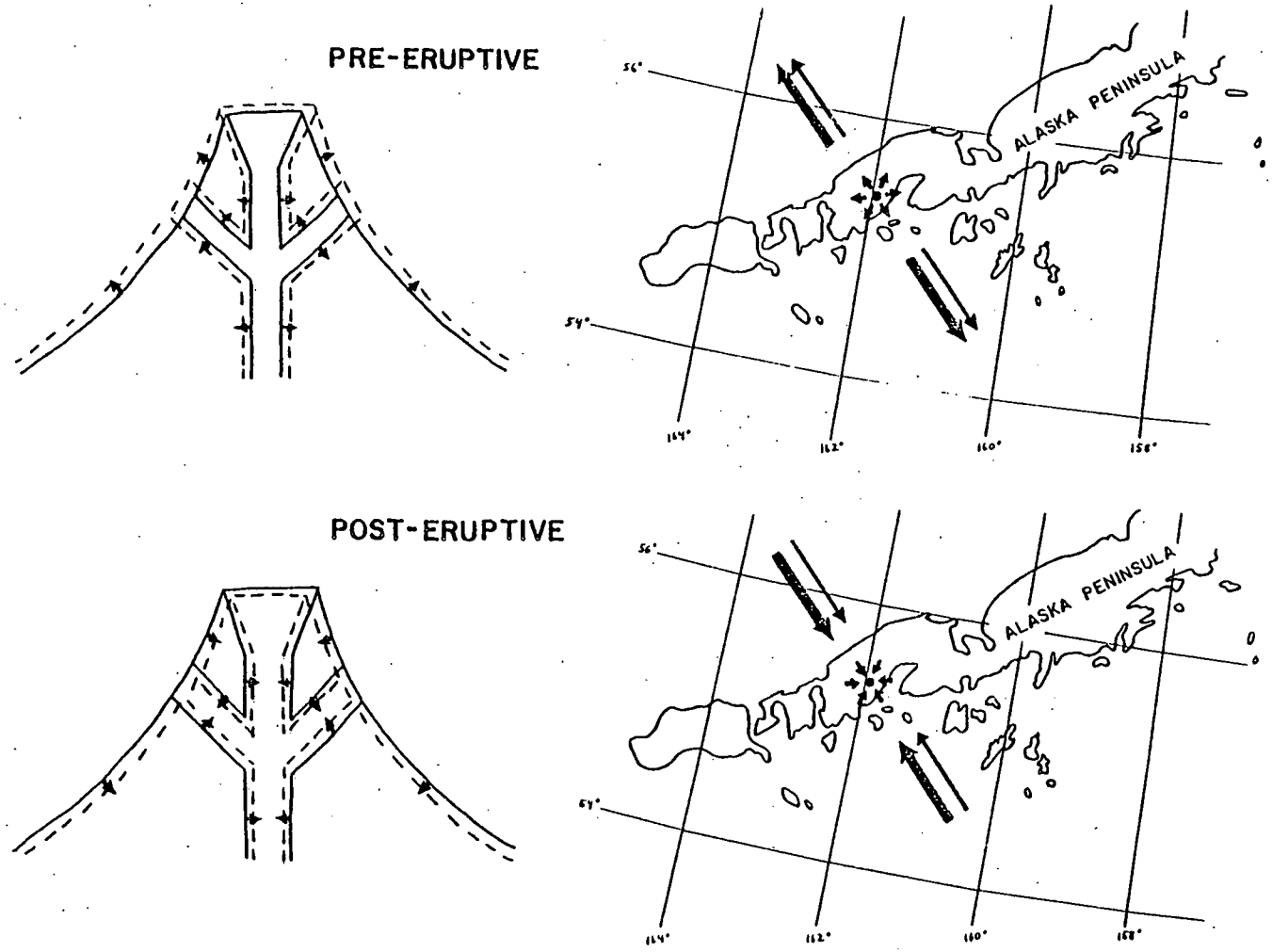

Figure 13. This figure schematically illustrates on the left-hand side the forces within the volcanic conduit system as excerted by the internal magmatic processes and on the right-hand side by both the internal magmatic process (radial pattern around Pavlof Volcano on Alaska Peninsula) and tidal and ocean-loading processes (large arrows) in the direction across the strike of the Aleutian arc. Note that for the pre-eruptive phase (upper two sketches) the inflation-induced expansion-stresses in the volcano are sympathetic with the high-tide stresses (corresponding to solid-earth volumetric extension), and for the past eruptive phase (lower two sketches) the deflation-induced stresses in the volcano are sympathetic with the low tide stresses (corresponding to solid-earth volumetric contraction).

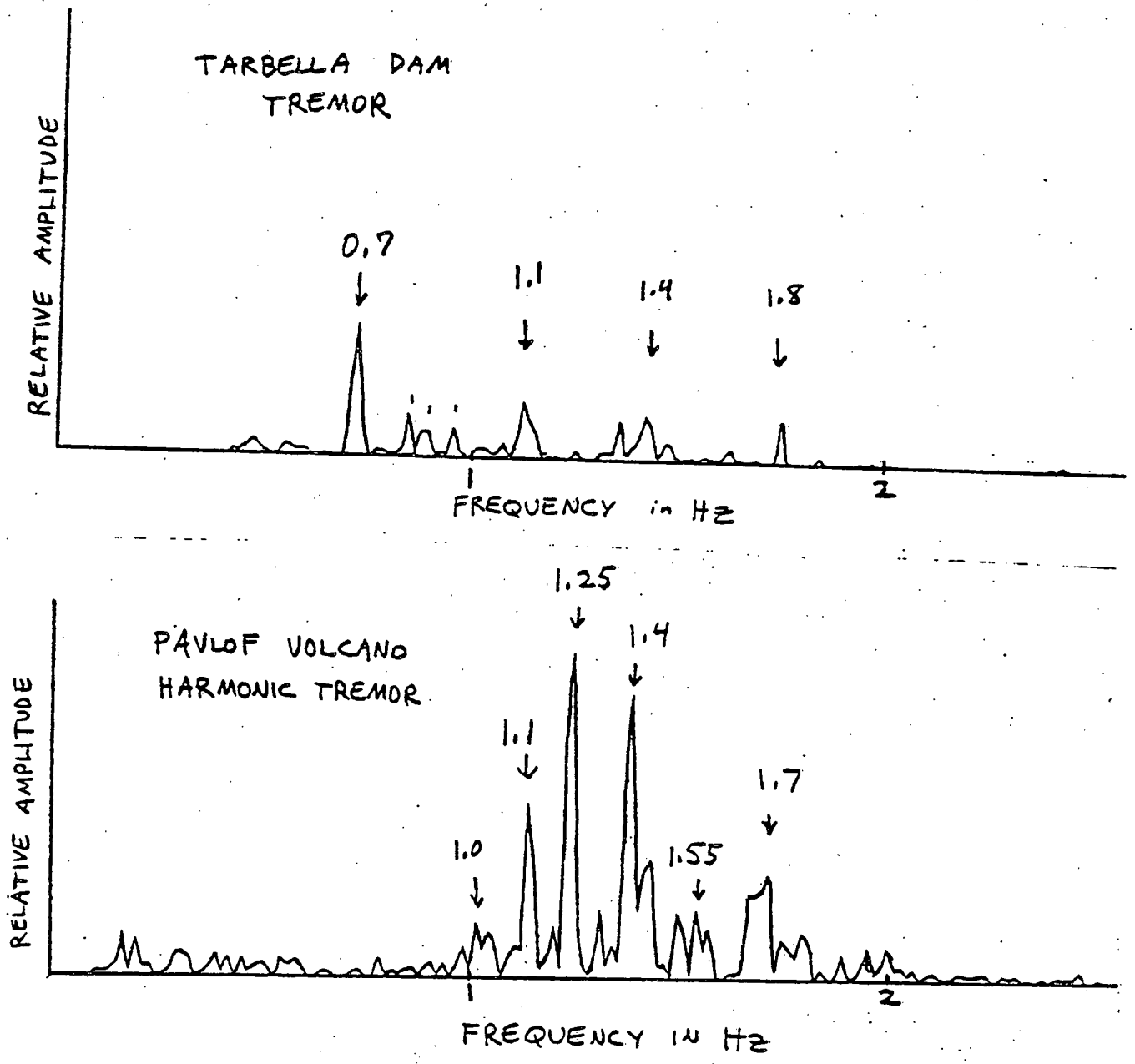

Figure 14. Discrete Fast Fourier Transform spectral analyses of signals from Tarbela Dam (Pakistan) and Pavlof Volcano (Alaska). Each plot shows the spectrum from one minute of record. Note the evenly spaced peaks in each spectrum, corresponding to standing waves of different modes set up in organ pipe-like resonators. The pipes are outflow tunnels at Tarbela dam and magma conduits at Pavlof Volcano.

7/4, 3/2, 9/4, 5/2, etc., but poorly recorded lower frequencies (including the fundamental modes). We infer that the source excites predominantly higher frequency modes.

Several mechanisms are suggested for exciting oscillations within the conduit that cause harmonic tremor: 1) intermittent flow of magma through the pipe, 2) conduit extension/contraction, and/or 3) nearly continuous explosions. The inferred length of the tube depends on the velocity of P-waves in magma; reported values of 0.3-2.0 km/sec yield values for the conduit length of 0.5-3.2 km.

D. Magma Chamber Study. Some new data have been obtained for the study to determine the size of a magma chamber under Pavlof volcano. The study involves the detection of travel time residuals and amplitude attenuation for ray paths of earthquake waves which travel through the root zone of Pavlof. A similar type of study by Iyers [1979] showed the presence of a low velocity zone under Yellowstone Park. The installation of our new, event-triggered tape recording system whose analog records can be digitized in an automized process has greatly enhanced this study. The resolution of P and S phases is much higher on the new recording system, and the timing system is much more accurate (1/100 sec). Preliminary results of several large (M 3-4) earthquakes in the Shumagin Islands region indeed show systematic travel time residuals for ray paths which travel through the root zone of Pavlof. We are now awaiting a sufficient amount of such high-accuracy data from the new system to "X-ray" a large crustal volume beneath Pavlof volcano.

E. Fuego and Pacaya Volcanoes. Pacaya volcano, Guatemala, is quite similar to Pavlof in its eruptive behavior [Eggers, 1979], while Fuego is more like Mt. St. Helens. The former have mild explosions and strombolian

eruptive behavior, while the latter have mainly Plinian eruptions. We are studying the short term cycles of seismic activity at each of these volcanoes using standard seismological methods, such as histograms of seismicity, earth tidal correlation studies, calculation of b-vaues, and frequency analyses. We expect an integrated approach to volcano seismicity will allow us to detect the common features of subduction zone volcanoes and their geothermal potential and hazardous properties.

F. Mt. St. Helens b-values. Figures 15 and 16 show examples of b-value plots calculated for two subsets of the Mt. St. Helens earthquake sequence. These plots demonstrate that several physical mechanisms are acting to produce earthquake signals. Further details of this study are given in the abstract (Appendix II) of a talk given at the fall 1980 PNAGU Meeting.

Stress Drops

Estimates of stress drops of earthquakes are important because the ground acceleration produced by an earthquake of a given moment is dependent upon the stress drop [Hanks and Johnson, 1976]. Also if one can assume high stress drop earthquakes are an indicator of a high level of regional stress, the location of these earthquakes should help in identifying areas under high tectonic stress, and thus likely sites of great earthquakes in the near future.

Last year we reported source parameters for four earthquakes in the Eastern Aleutians. Using the methods described in last year's report, we estimated the stress drop for 10 more moderate earthquakes in the same region (Figure 17). The data used were short-period WWSSN film chips and

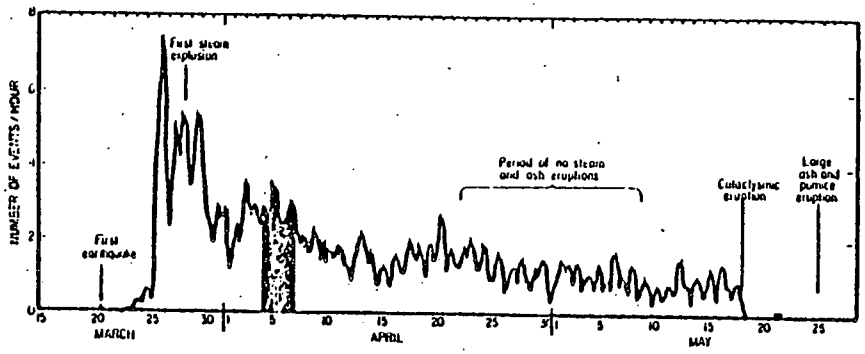

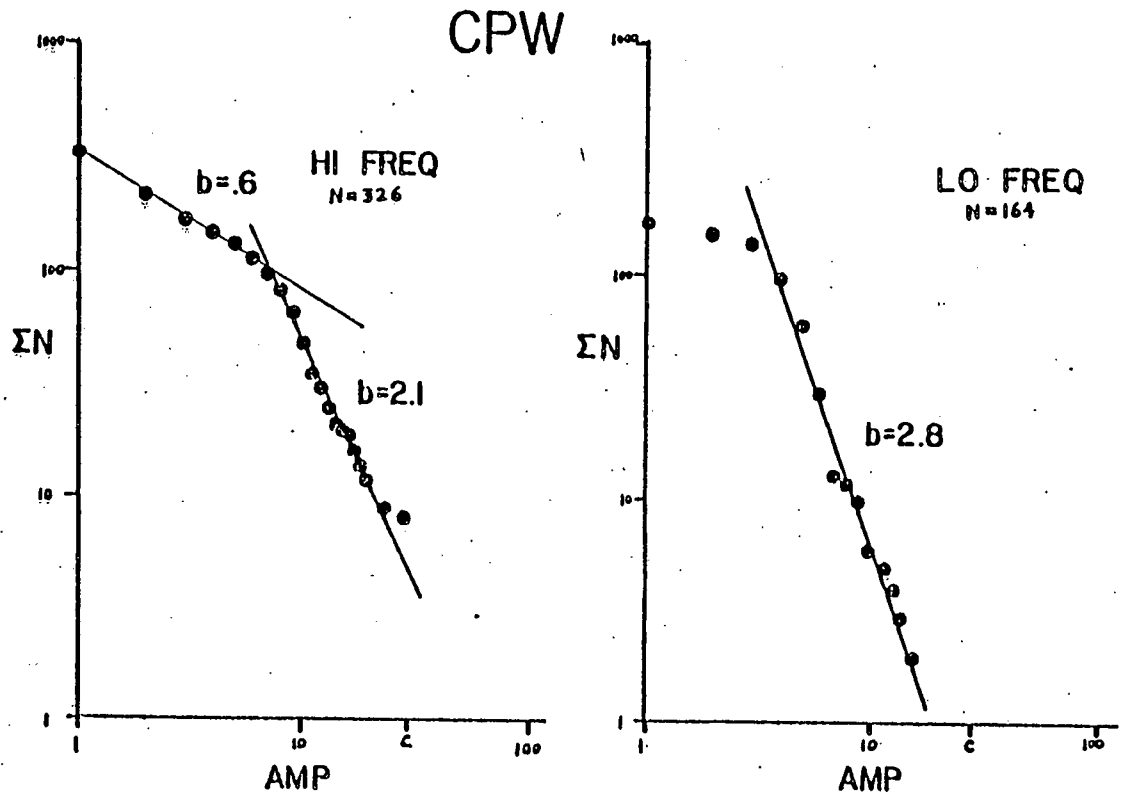

Figure 15. B-value plots for April 4 - April 6, 1980 volcanic earthquakes from Mt. St. Helens. The distinct break in slope on the high frequency plot (left) is interpreted as indicating that two physical mechanisms are acting; the break in slope represents a kind of threshold value*. Vertical axes on both plots are cumulative number of events, horizontal axes are log peak to peak signal amplitude.

*Low frequency events for this time period do not show a statistically reliable break in slope.

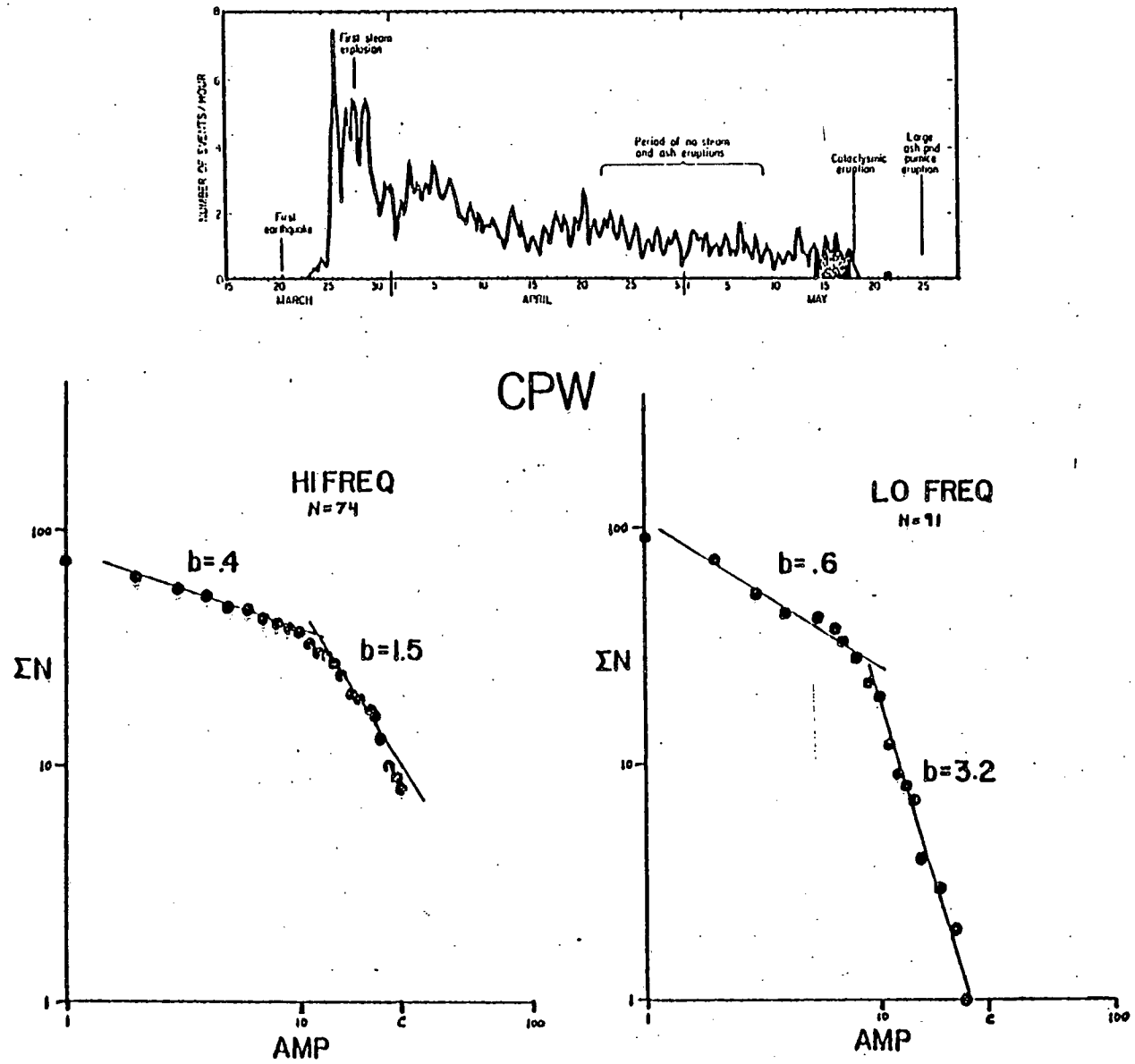

Figure 16. B-value plots for May 14 - May 18 volcanic earthquakes from Mt. St. Helens. Both high frequency (left) and low frequency (right) events show a break in slope, again indicating that two physical mechanisms are acting.

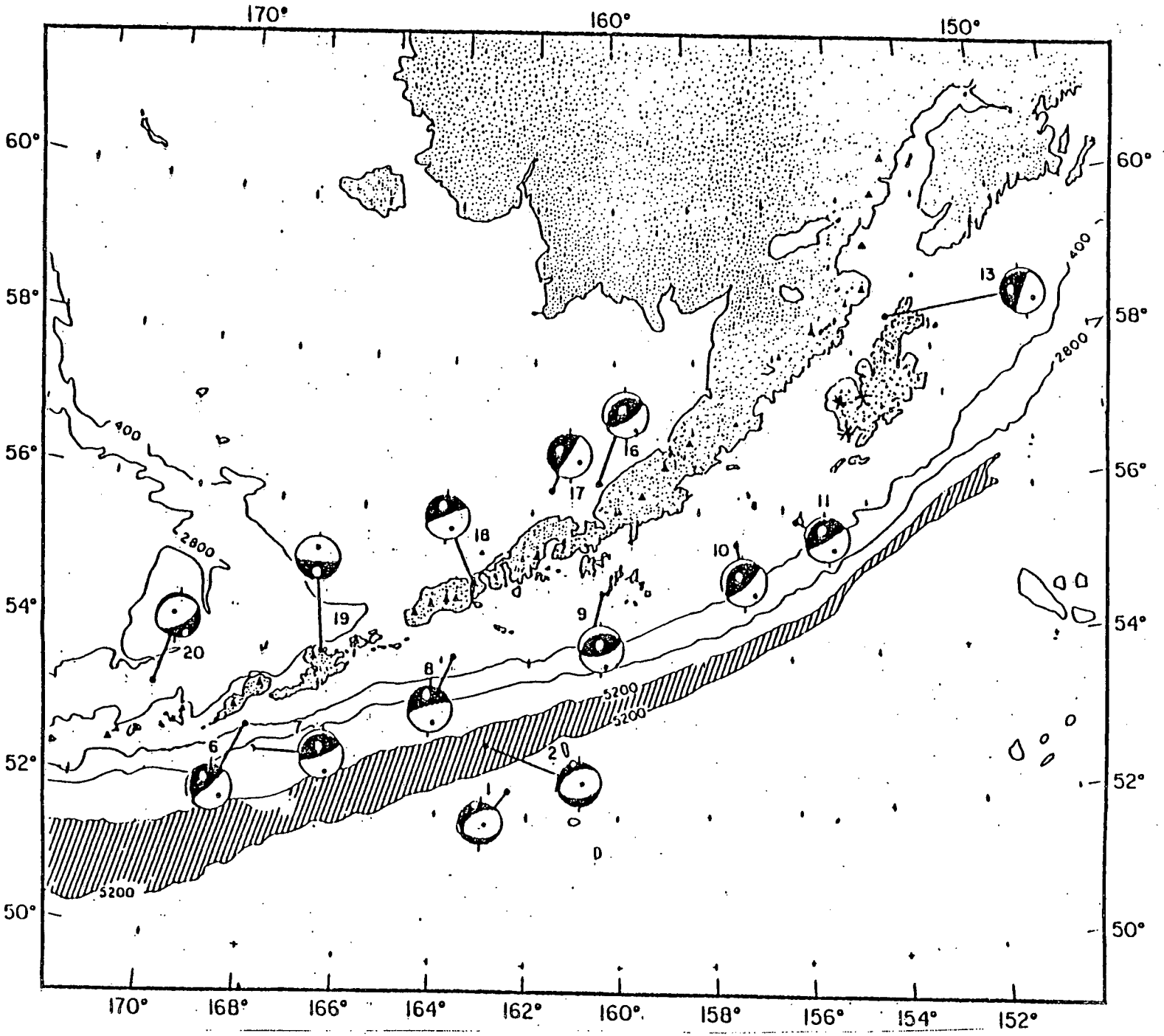

Figure 17. Focal mechanisms (Davies et al., 1980) of earthquakes analyzed in this study.

records from a broadband instrument located in Palisades, New York. One factor which was not taken into account last year was attenuation. More recently we assumed that anelastic attenuation was represented in frequency domain by

$$Q(w) = \exp\left[-wt^* + \frac{iwt^*}{2}\left(\ln\frac{w}{w'} - 2\right)\right]$$

where w is the angular frequency, w' is the Nyguist frequency, and t* is a measure of the energy loss per cycle [Carpenter, 1966]. Then one can form an inverse Q operator, transform it into time domain, and apply it to the data to take out the effects of attenuation. Figure 18 shows the plots of velocity and velocity convolved with the inverse Q operator for the data used in analyzing event 9. One notices that the convolution is very unstable to noise and completely destroys much of the shape. But the initial "rupture phase" stays coherent, and since it is the slope of this "rupture phase" which is used to calculate dynamic stress drop, the noise later on in the signal should not offset our estimates of stress drop.

The t* used in this study was taken to be 0.6 for all the events. Published values of t* range from 0.1 to 1.0 [Der and McElfresh, 1975; Anderson and Hart, 1978; Sommerville et al., 1976]. A different t* could change the absolute value of stress drop by a factor of 2 or 3, but it would not change the relative values obtained for the earthquakes in this study.

The dynamic stress drops calculated for the 14 events are tabulated in Table 1. Despite the scatter in the data, there are significant differences in the dynamic stress drops among these earthquakes. The scatter in the results could partly be due to local conditions at the site and receiver. The shallow earthquakes occur in areas which are probably more complex

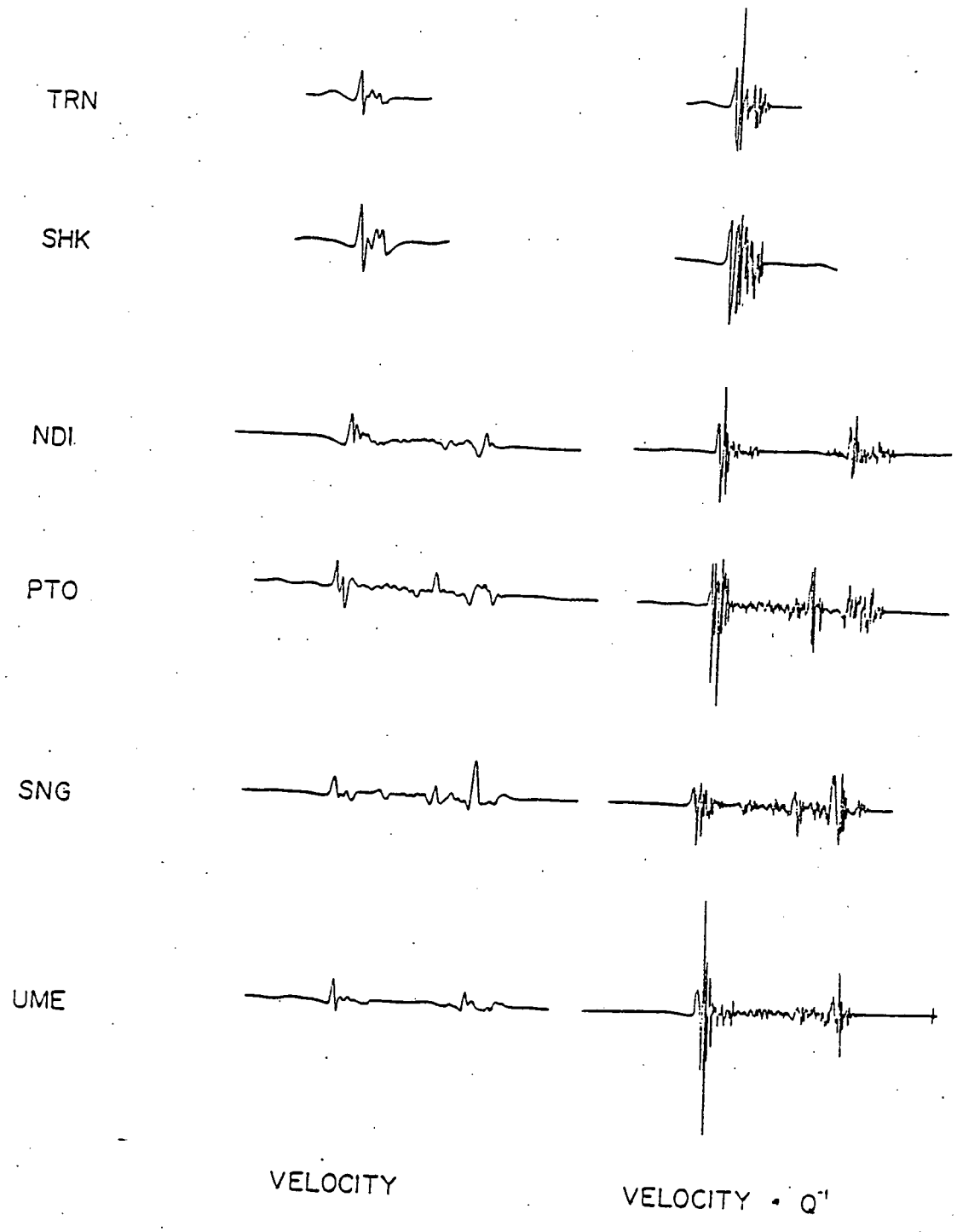

Figure 18. Deconvolved velocity plots for event 9 are shown in the first column. The second column is a convolution of the velocity plots with an inverse Q operator ($T^* = 0.6$). Note that the rupture phase stays coherent despite all the noise in the healing phase. The vertical scale for the second column is three times greater than the first column so that the convolution with the inverse Q operator increases the amplitude of the rupture phase by about a factor of 3.

TABLE 1

Event 1	6/20/69	Depth 7 km	m_b = 5.8
	DUG	83 bars	
	NDI	55 bars	
	PTO	93 bars	
	SNG	105 bars	
	PAL	50 bars	

Event 2	10/13/72	Depth 9 km	m_b = 6.0
	DUG	42 bars	
	NDI	178 bars	
	PTO	115 bars	
	IST	161 bars	
	GOL	58 bars	

Event 6	11/12/69	Depth 50 km	m_b = 5.5
	DUG	13 bars	
	NDI	18 bars	
	TUL	6 bars	
	GOL	6 bars	

Event 7	7/6/67	Depth 49 km	m_b = 5.9
	PTO	47 bars	
	IST	44 bars	
	TRI	31 bars	
	PAL	26 bars	

Event 8	5/29/73	Depth 17 km	m_b = 6.1
	DUG	163 bars	
	NDI	256 bars	
	PTO	221 bars	
	SNG	109 bars	
	TUC	240 bars	
	STU	286 bars	
	LON	394 bars	
	GOL	250 bars	

TABLE 1 (con't.)

Event 9	4/6/74	Depth 40 km	m_b = 6.0
	NDI	117 bars	
	PTO	154 bars	
	SNG	150 bars	
	UME	102 bars	
	TAN	179 bars	
	IST	37 bars	
	PAL	109 bars	
	SHK	212 bars	
Event 10	2/13/79	Depth 24 km	m_b = 5.8
	PAL	65 bars	
Event 11	2/6/64	Depth 15 km	m_b = 6.1
	PAL	167 bars	
Event 13	12/22/64	Depth 40 km	m_b = 6.4
	PAL	85 bars	
Event 16	11/25/71	Depth 136 km	m_b = 5.5
	KTG	47 bars	
	GOL	44 bars	
	GSC	18 bars	
Event 17	6/10/68	Depth 170 km	m_b = 5.5
	DUG	26 bars	
	TUC	50 bars	
	LON	23 bars	
	GOL	77 bars	
	QUE	17 bars	

TABLE 1 (con't.)

Event 18	9/4/71	Depth 115 km	m_b = 5.7
	DUG	21 bars	
	NDI	73 bars	
	PTO	78 bars	
	KBS	84 bars	
	UME	45 bars	
	PMG	50 bars	

Event 19	4/21/72	Depth 100 km	m_b = 5.8
	NDI	12 bars	
	PTO	27 bars	
	KTG	14 bars	

Event 20	4/5/71	Depth 150 km	m_b = 5.8
	NDI	47 bars	
	SNG	68 bars	
	KTG	76 bars	
	UME	60 bars	

structurally. This may account for the more complex pulse shapes of the shallow events. No corrections were made for structures at the source, such as the dipping slab (Figure 8) which could significantly offset shape and amplitude of the waveform [Davies et al., 1980].

Figure 19 is a plot of dynamic stress drop versus depth. Lines connect points which represent stations used in analyzing the same event. Although this data set is too small to represent a fair statistical sampling, we believe it indicates that differences in stress drop occur as a function of location. At depth of 100-200 km where no great earthquakes are known to occur the stress drops of these moderate earthquakes fall in the range of 10-75 bars. The very shallow normal-faulting earthquakes near the trench seem to have in the average somewhat higher dynamic stress drops than the Benioff zone events. Whether this high stress is a local feature of this particular arc segment or occurs consistently along the entire arc is not known at this stage of the study.

The earthquakes within the main-thrust-zone (depth 15 to 50 km) show the greatest variation in dynamic stress drop along the arc. This fact is illustrated in Figure 20. Note that the two low-stress earthquakes in this category fall within the aftershock zone of the 1957 event; also the earthquake which appears to have the highest stress drop is the one which occurred at the edge of the 1964 rupture zone and one month prior to the 1964 event. Event 7 is located in the 1938 aftershock zone, and occurred at times sufficiently long after the great 1938 event so that the intermediate value of stress drop may represent the stress accumulations of an area midway in the development of an earthquake cycle. These apparently consistent stress variations for moderate-size earthquakes in the main thrust zone suggest that dynamic stress-drop estimates from such events

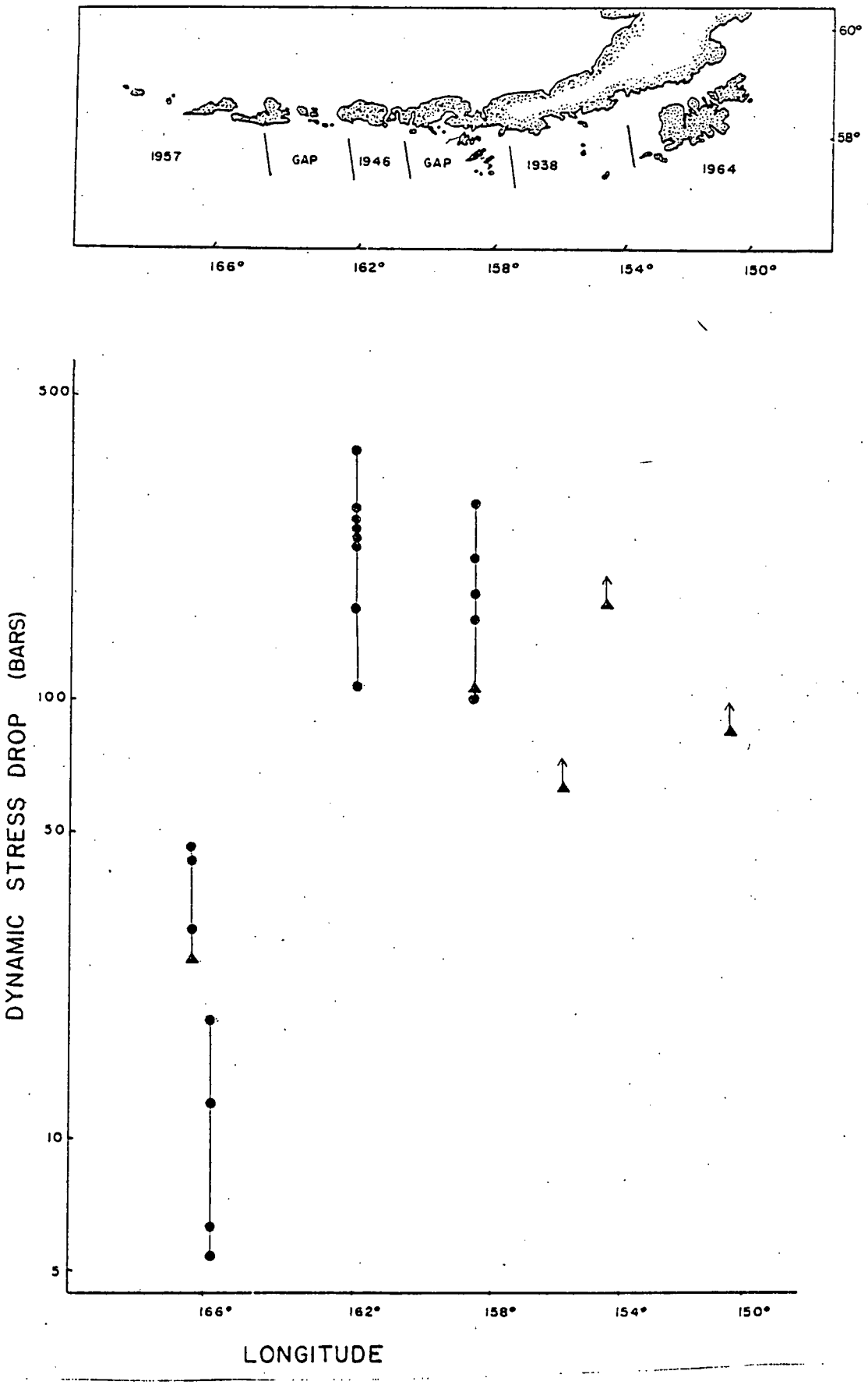

Figure 19. Plot of dynamic stress drop versus depth. Note the wide range of stress drops for the earthquakes at depths of 15-50 km.

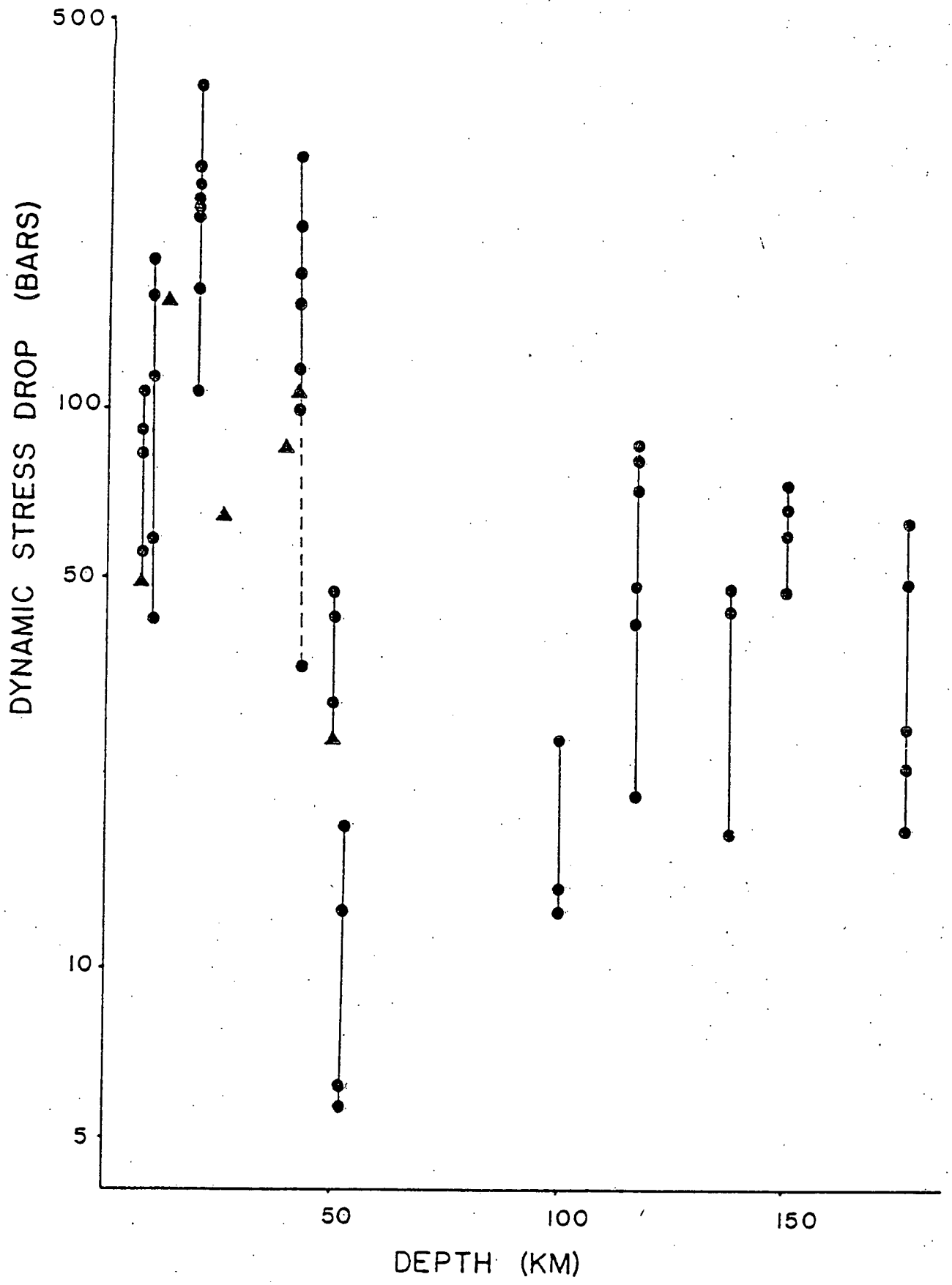

Figure 20. Dynamic stress drop plotted against longitude. The lowest stress drop earthquakes are located within the 1957 rupture area. High stress drop earthquakes are located within or at the edges of gaps.

may provide some indication of the level of stress that has been attained within different segments of a subduction zone. Higher stress drops are observed for regions that appear in time close to the occurrence of a great earthquake. In addition it appears that shallow interplate earthquakes and intermediate-depth intraplte earthquakes (within the subducting slab) have distinctly different stress drops.

Conclusions. We have shown that there is a difference in stress drops of earthquakes in this region. This difference is important in identifying areas which may be under high tectonic stress and thus likely sites of large or great earthquakes in the near future. The breaking of high stress asperities may also be a part of the rupture process in all earthquakes, so the distribution of high and low stress drop events is important in predicting strong ground motion from earthquakes of all sizes.

Crustal Deformation

The work on crustal deformation in the Shumagin Islands presently takes two forms: (1) annual levelling of short level lines, and (2) annual distance measurements using laser instruments.

1. Crustal tilting. We now have eight level lines (Figure 21) at various locations in the islands, ranging in length from 500 m to 1200 m. L1 and L5 have been measured since 1972, L2 since 1977, L6 since 1978, L3 since 1979 and L6, 7 and 8 were installed in 1980. In Figure 22 we show the results from lines L1, 2, 3, and 6. L5 is not considered because of problems with unstable benchmark installations. Figure 22 shows the height difference between the ends of each line as a function of time. Each line is oriented approximately NW-SE, perpendicular to the Aleutian

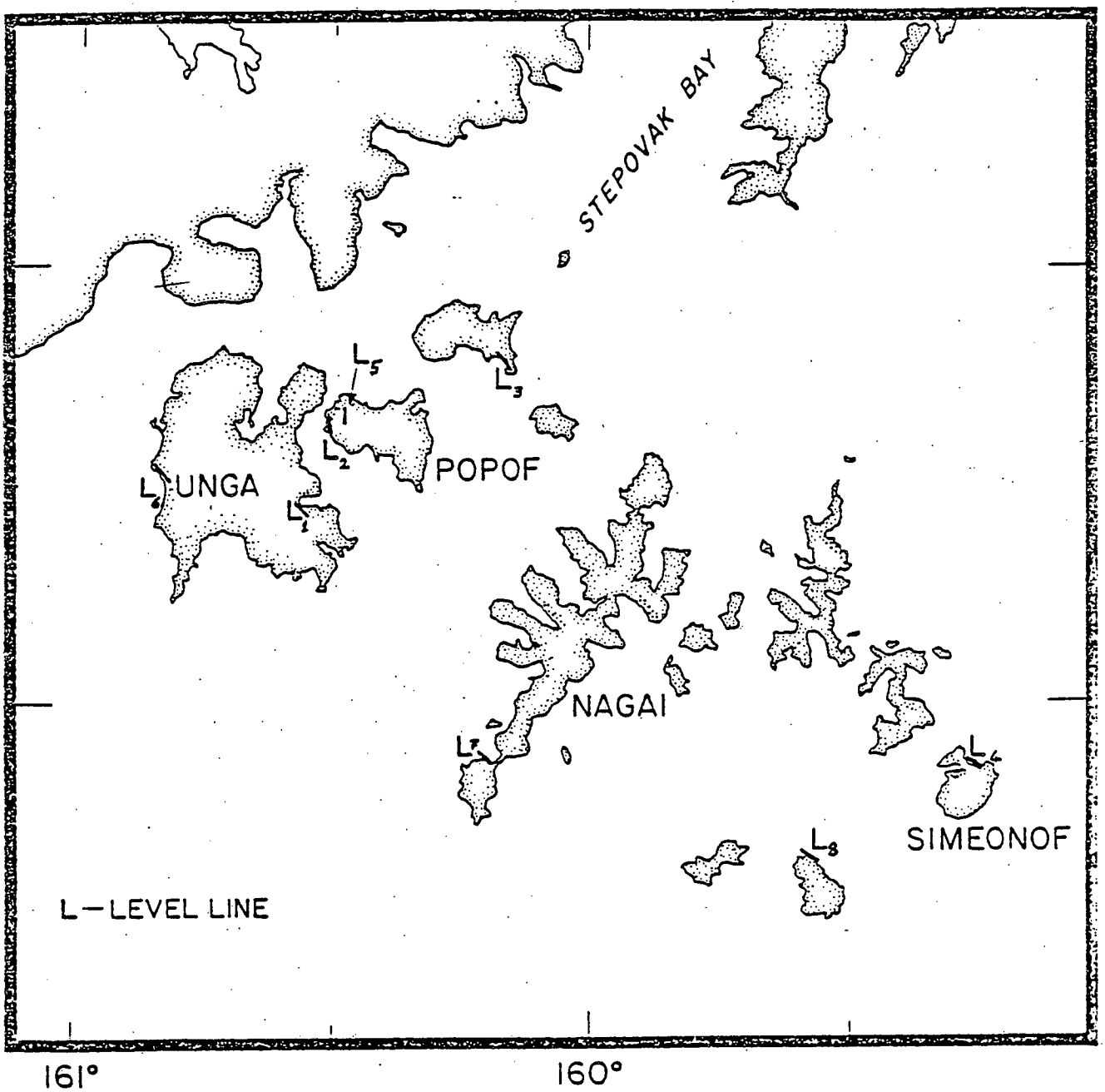

Figure 21. The Shumagin Islands showing our present network of levelling lines. Lines L1 and L5 were installed in 1972; L2 in 1977; L4 in 1978; L3 in 1979; and L6, L7 and L8 in 1980. The approximate position and azimuth of the lines is shown.

Figure 1

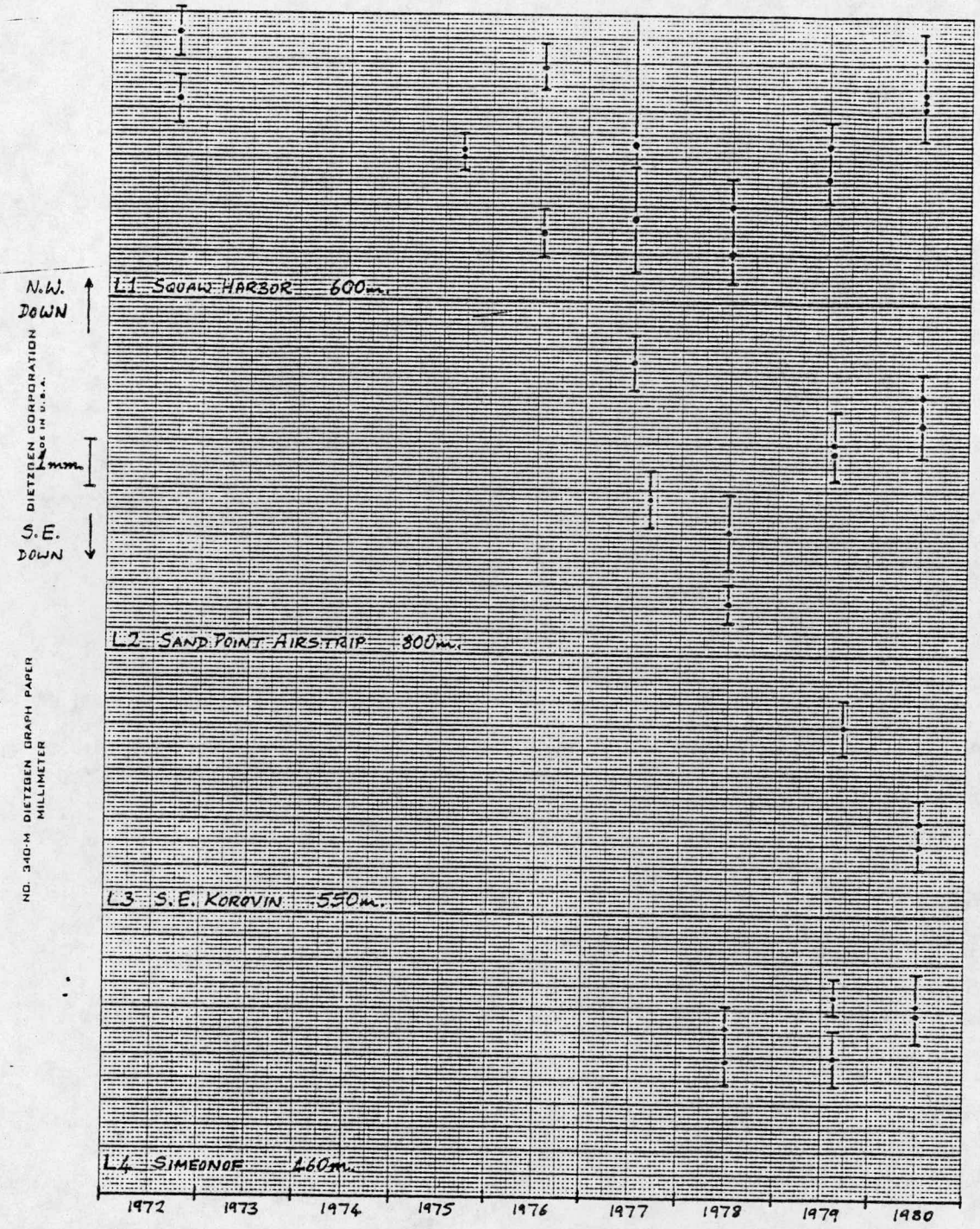

Figure 22. Levelling results since 1972. The graphs show the height difference between the ends of each line as a function of time. The location and length of the line are shown at the bottom left of each graph. A falling trend represents tilting down to the SE; a rising trend, tilting down to the NW. The two measurements shown for each year represent the forward and backward runs of levelling. The error bars are 1 standard deviation based on the scatter in the readings to the levelling shafts.

trench axis. The graphs are drawn such that a falling trend with time represents tilting down to the SE and a rising trend tilting down to the NW. Note that the graphs are not normalized to the length of the level line; if they were, the trend on the graphs of the shorter lines would be relatively steepened. Two points are normally shown for each year - these represent the forward and backward rms errors of leveling. The errors as shown are those for one standard deviation, based on the scatter in the readings of the levelling staffs along the line.

We point out the apprent agreement between the trends on lines L1, 2, and 6 between 1978 and 1980. Though none of the trends are significant at a high confidence level when taken individually, taken together they do give credence to the trend being real (tilting down towards NW). The disagreement on line L3 cannot be quantified - the line was measured in only one direction in 1979 so there is no way to check whether this measurement might have been in error.

The change of trend on line L1 between 1972-8 (SW down) and 1978-80 (SW up) is weakly supported by the similar change on line L2. If we assume the change in tilt polarity is real, it might be explained by a slip event propagting along the upper surface of the sinking slab beneath the islands. The tilting down towards the trench between 1972 and 1978 represents a phase of loading of the upper plate by the sinking slab. The slip event then causes the upper plate to become unloaded and thus recover some of the bending in the upper plate which took place during the loading phase. This, of course, is only one, highly speculative, interpretation of the data.

2. Trilateration measurements. At our instigation, Dr. John Savage of the USGS started in 1980 a network of high precision geodolite distance

measurements between the various islands and the mainland. This network will be repeated and extended next year,and will eventually give a measure of the long-wavelength strain field accumulating in the region.

We have also measured four small-scale quadrilaterals, having sides between 1 and 8 kilometers in the inner Shumagins. We use a laser ranger which gives a precision of several millimeters, and we can thus expect to see strain changes of order 10^{-6} or larger; this will most likely be useful in determining coseismic deformation, but may also be useful in a predictive mode if large premonitory strains occur.

Technical Accomplishments

1. Network Status, August 1980 (following summer fieldwork)

There are now three networks operated by L-DGO in the eastern Aleutian arc-Pribilof Islands region (Figure 23): the Pribilof Network, recorded at St. Paul (SNP); the Unalaska Network, recorded at Dutch Harbor (DUT); and the Shumagin Network, recorded at Sand Point (SAN). The Pribilof and Unalaska Networks have been established largely with the support of the NOAA/BLM OCSEA Program for the purpose of seismic hazards evaluation. The Shumagin Network and its subarray on Pavlof Volcano was established largely with support from the DOE and some initial equipment from the USGS. The original purpose of the Shumagin Network was to provide data for tectonic studies with some geothermal studies being added when the Pavlof subarray was installed. The data from all of these networks can, of course, be used for both hazards and tectonic studies; indeed, there is a synergistic benefit in carrying out these studies simultaneously.

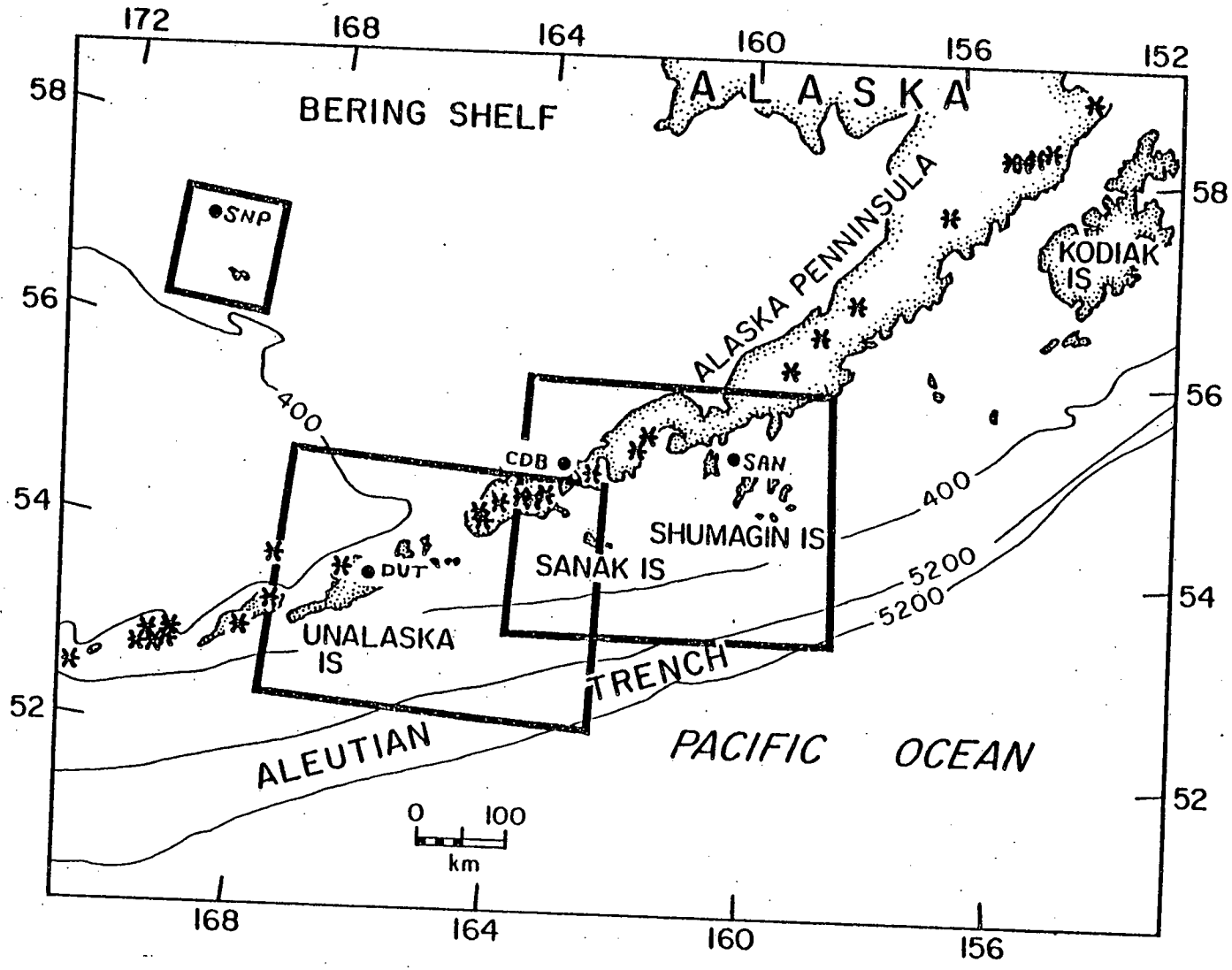

Figure 23. Location map for study area. Four logistic bases are shown at St. Paul (SNP) in the Pribilof Islands, Dutch Harbor (DUT) on Unalaska Island, Cold Bay (CDB) on the Alaska Peninsula, and Sand Point (SAN) in the Shumagin Islands. The three boxes around SNP, DUT, and SAN indicate, respectively, the outlines of the maps shown in Figures 24, 25, and 26. To relate Figures 25 and 26, note that Sanak Island is shown in both.

The Pribilof Network (Figure 24) consists of two remote stations and the local station at St. Paul. The sensors at the local station (SNP) consist of a short- and a long-period vertical seismometer. The sensors at the two remote stations are short-period vertical seismometers.

The Unalaska Network (Figure 25) consists of three remote seismic stations, one repeater station and the local station at Dutch Harbor. The sensors at the local station (DUT) consist of three orthogonal short-period seismometers, a long-period vertical seismometer and an orthogonal set of strong-motion accelerometers. The seismometers at the remote stations are all short-period vertical instruments.

The Shumagin Network (Figure 26) consists of 13 remote stations plus 10 stations in the Pavlof Volcano subarray, three repeater stations and the local station at Sand Point (SAN). Each remote station has a single, short-period vertical seismometer except Chernabura (CNB) which is now a three-component station. Within the region of the Shumagin Network there are now nine strong-motion accelerographs (see Figure 26 and the discussion below), six of which are co-located with remote stations of the network. Sensors local to the recording center at Sand Point (SAN) consist of orthogonal sets of short- and long-period seismometer, and strong-motion accelerometers.

The three component station at Chernabura was established following a decision to begin a program of upgrading a subset of the network by adding horizontal seismometers. The horizontal components yield important information that is not obtainable from a single, vertical component regarding the arrival times of the shear and converted waves (see section by Reyners and Coles); these arrival times can strongly constrain the location of the hypocenters of earthquakes within the network and provide an almost unique

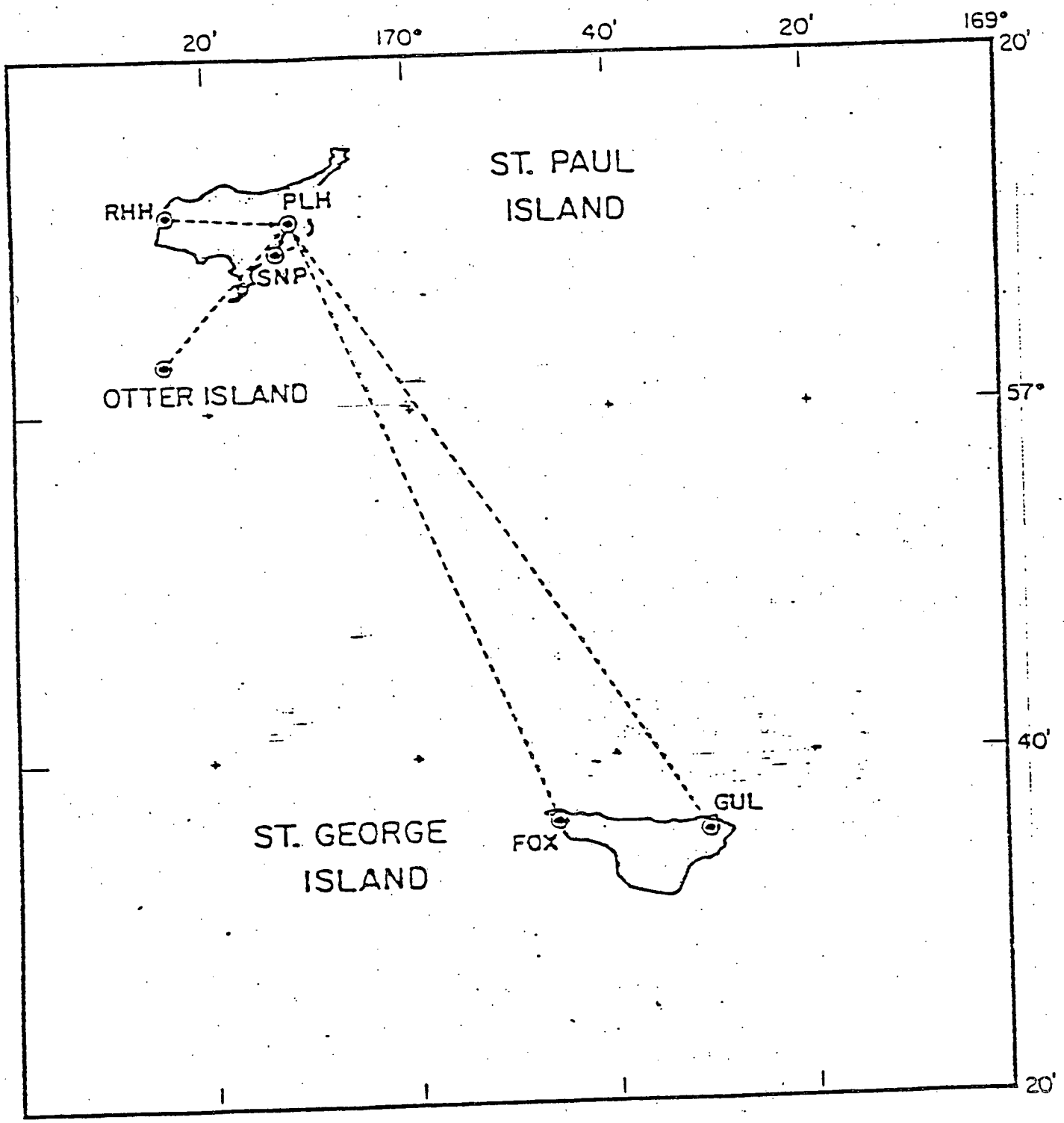

Figure 24. Previously proposed (to NOAA/BLM) Pribilof Islands Network (see Figure 23 for location). Installed this summer were RHH and PLH. The three short-period seismic signals from RHH, PLH and SNP are recorded on a triple-drum helical recorder in the NWS observatory on St. Paul Island.

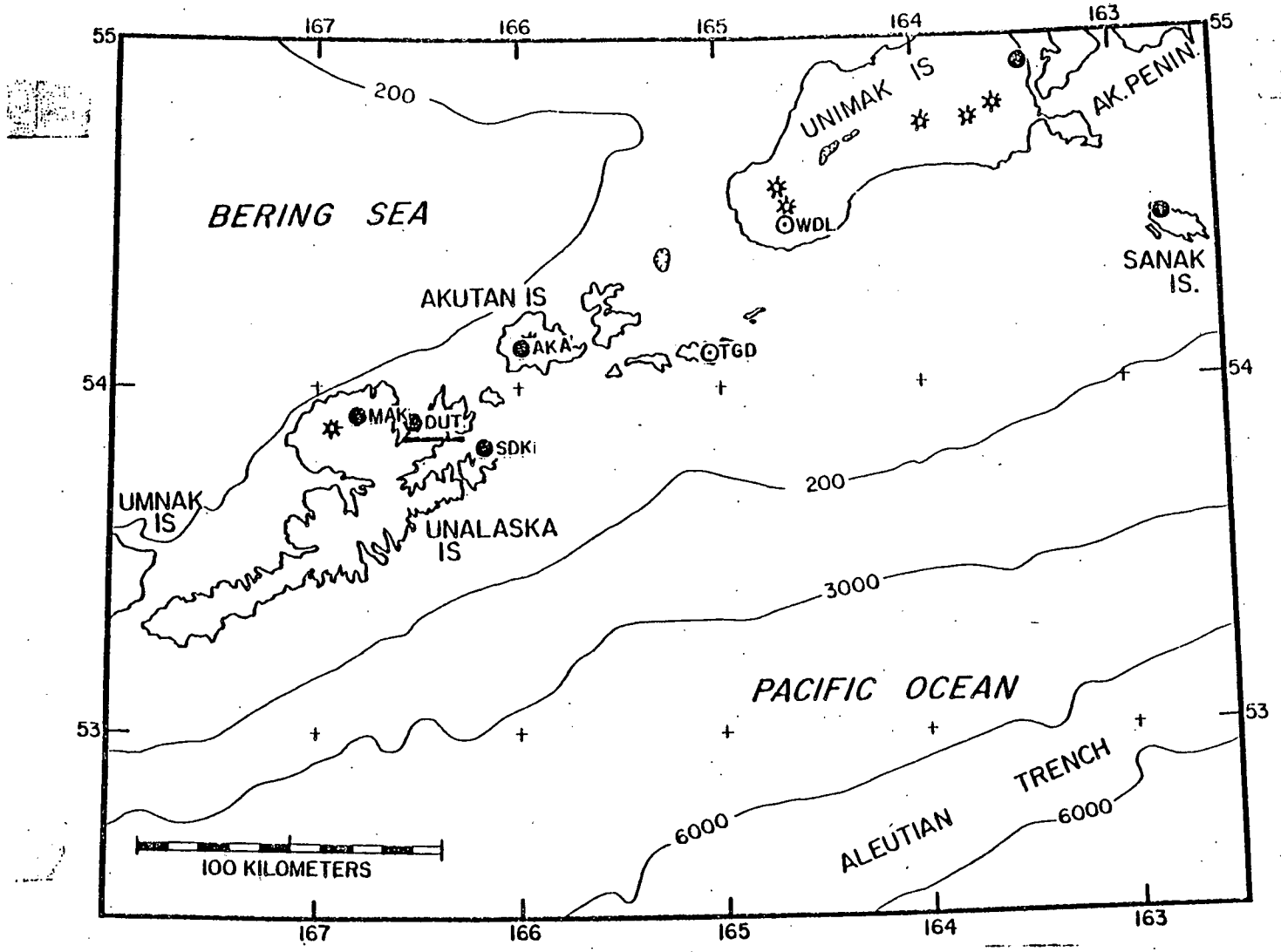

Figure 25. Unalaska Network (see Figure 23 for location). Remote stations (MAK, SDK, AKA) are shown by a filled circle, stations planned but not installed (TGD and WDL) due to weather and mechanical problems are shown by the circles enclosing a dot. The two filled circles in the upper right corner are the stations False Pass (FPS) and Sanak Island (SNK) of the Shumagin Network. The recording center for the Unalaska Network is in Dutch Harbor (DUT) shown by a filled hexagon. The sensor at each of the remote stations is a single, vertical seismometer of 1 Hz natural frequency. At DUT there are three orthogonal seismometers at 1 Hz, one vertical at 15 sec and a Kinemetrics SMA-1 strong-motion accelerograph (indicated by the heavy line under the designator code DUT). In addition to the usual short-period mode, the orthogonal set is also recorded in an intermediate period mode which is designed to span the band from 20 to .25 seconds period and to be intermediate in magnification between the short period and the strong-motion systems. All of the signals (except those of the SMA-1) are event-detected and recorded on analog magnetic tape. Two helicorder records are made to continuously monitor the system. The magnetic tapes are digitized and processed at L-DCO using the USGS PDP 11/70 data analysis sytem.

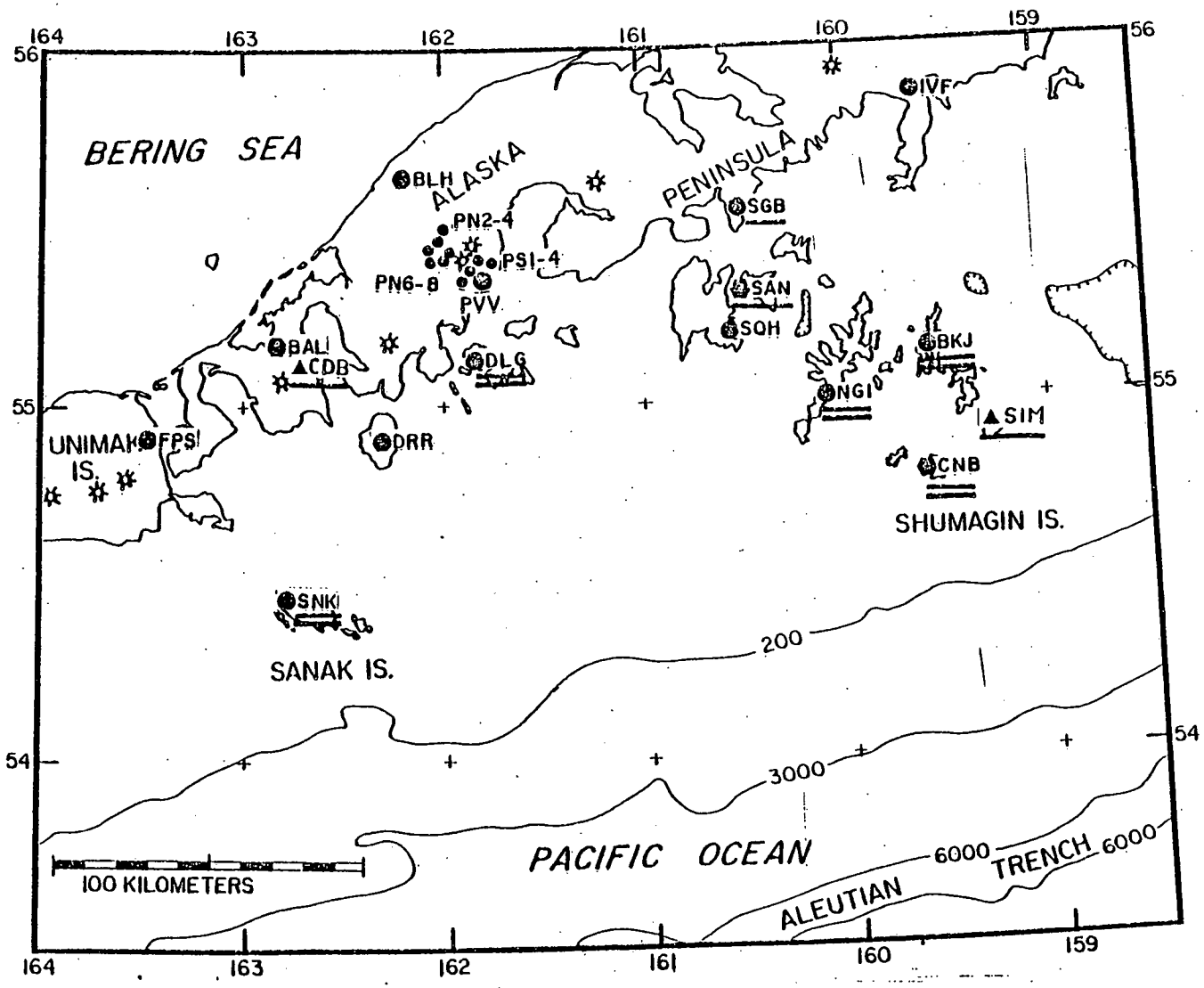

Figure 26. Shumagin Network (see Figure 23 for location). Remote stations with a single, vertical geophone are shown with filled circles. Stations with three orthogonal seismometers (CNB and SAN) are shown with a filled hexagon. Network stations with SMA-1 strong-motion accelerographs (SNK, NGI, DLG, SGB, BKJ, SAN, CNB) are indicated by the heavy line under the designator code. Those with double underlining transmit an SMA trigger signal: when one of these SMA's is triggered, a tone is sent via the VHF telemetry system to a detector at SAN which turns on the tape recorder. The triangles at SIM and CDB indicate SMA-1's unrelated to any network station. The SAN station has three orthogonal long period seismographs as well as the short and intermediate period system similar to that at DUT (see caption from Figure 25). Signals at SAN are recorded on an event detecting magnetic tape recorder, a Develocorder and 5 Helicorders; records from these devices are processed at L-DGO.

data set for interpreting first-order velocity discontinuities below the net. The location and nature of these discontinuities are important elements of a seismotectonic analysis of the subdution process in the Shumagin region.

Six new strong-motion accelerographs were installed this summer, bringing the total in the region to nine (plus one at DUT). These are all Kinemetrics 1g SMA-1's. Five of them (see Figure 26) are connected to the telemetry system so that a trigger signal allows us to know the exact time at which the SMA began recording a given earthquake. Most of the support for these instruments came from a USGS contract. This system has already recorded one m_b = 5.2 event just SW of Nagai (NGI).

Helicopter support was provided by the NOAA/BLM OCSEA Program. This support would cost about $100,000 from a private contractor and is vital to the maintenance of the number of stations in the Shumagin and Unalaska Networks. Maintenance of the remote stations requires about 30 days for a five person crew. The central recording stations require about two weeks of maintenance, three times per year by a two man crew.

2. Improvements made at the Central Recording Stations

Universal time receivers for the standard time broadcast via satellite have been installed at all three of the recording centers. These receivers provide local time automatically synchronized to Coordinated Universal Time to within a few milliseconds. This obviates the need to maintain time corrections for the data collected at a particular site and, more importantly, eliminates the need to collect time-correction information (like the date) from the local station operators, removing the

sseemingly inevitable confusion between local and CUT time. A separate, local clock (TS250, eg.) is maintained at each recording center in case the receiver or the satellite fail.

Intermediate period seismographs were installed at Sand Point and Dutch Harbor. Two three-component sets of Baby-Benioff seismometers (1 Hz natural frequency) were provided by L-DGO to the Alaska-Aleutian project; one set each was installed in the vaults at SAN and DUT. The signals from these instruments are conditioned by two-channel filter-amplifier-VCO units newly built by the L-DGO seismology group. One channel provides a standard short-period output (am and fm) and the other, an intermediate period (IP) output (am and fm). The IP output is designed to cover the range 20 to .25 sec and to be intermediate in gain between the short period and strong motion systems (see Figure 27). The IP system is intended to provide data critical to the stress-drop and waveform studies described above by J. Mori. The amplitude-modulated (am) outputs can be recorded on the Develocorder or on a Helicorder, whereas the frequency-modulated (fm) outputs are mixed onto the event-detecting magnetic tape recorder described below.

Event-detecting, magnetic tape recording systems were installed at both Sand Point and Dutch Harbor. The event-detector consists of one to eight signal-detector modules and a logic unit which is based on a programmable-read-only-memory (PROM) chip. The signal-detectors switch to an "on" state whenever the short-term average (STA) of the signal exceeds the long-term average (LTA) by some selectable level. The PROM can be programmed so that any logical combination of states of the signal-detectors can cause the event-detector to declare an event and switch on the tape recorder (Figure 28). Two four-channel TEAC audio tape recorders

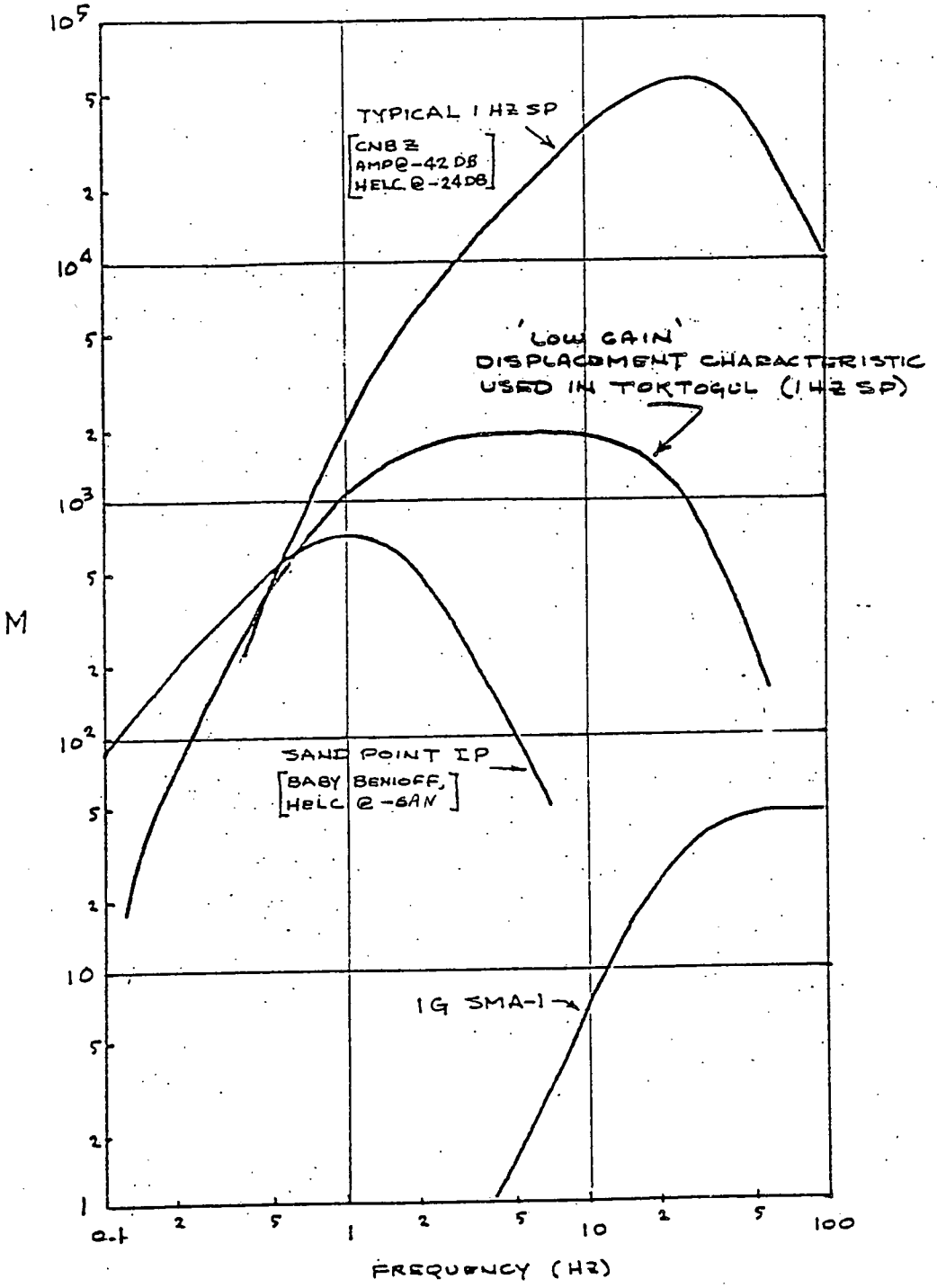

Figure 27. Comparison of the intermediate-period system to other seismographs. Response functions (magnification, M, vs. frequency) are shown for various seismographs: (1) the "typical 1 Hz sp" system is exemplified by the short-period station CNB (Figure 26) as recorded on a Helicorder; (2) the "low gain" system is not presently employed in the Alaska-Aleutian networks, is in use in the L-DGO Toktogul Network in the USSR; (3) the "Sand Point IP" system is the newly installed intermediate-period seismograph at SAN (and DUT; see Figures 25 and 26) as recorded on a Helicorder; (4) the "1G SMA-1" system is the Kinemetrics SMA-1 strong-motion accelerograph with sensitivity such that it will record on scale, accelerations up to 1g. Note that the IP system is intermediate in gain between the short-period system and the strong-motion system.

TRIGGER LOGIC FUNCTIONS
SAND POINT EVENT DETECTOR
1980 MARCH -

FUNCTION 1:	ANY ONE GROUP
FUNCTION 2:	ANY TWO GROUPS
FUNCTION 3:	ANY THREE GROUPS
FUNCTION 4:	ANY FOUR GROUPS
FUNCTION 5:	"STRONG EVENT"; ANY THREE GROUPS EXCEPT (F·G·H)
FUNCTION 6:	"WEAK EVENT"; ANY TWO CONTIGUOUS GROUPS, I.E.: A·B + A·C + B·C + D·E + D·F + D·G + D·H + F·G + G·H + F·H
FUNCTION 7:	SAME AS 6 EXCLUDING PAVLOF, I.E. F·G + G·H + F·H OMITTED
FUNCTION 8:	"GOOD STATION": SIGNAL DETECTOR A OR SIGNAL DETECTOR B OR ANY CONTIGUOUS GROUPS ON OTHER SIGNAL DETECTOR

Figure 28a. Table showing the eight (switch-selectable) logic functions stored in the PROM (programmable-read-only-memory) of the Sand Point event detector. The "groups" referred to in this table are sets of stations enclosed by the heavy lines in part (b) of this figure. For the event detector "group" means the signal detector representing a given group of stations; for example, in group F the signal from station SGB is input to signal detector F, that from NGI to G, and so on for the remaining groups of stations. If an event were to cause only signal-detectors F and G to switch "on" it would be recorded by the tape recorder only if one of logic functions 1, 2, 5, or 8 had been selected.

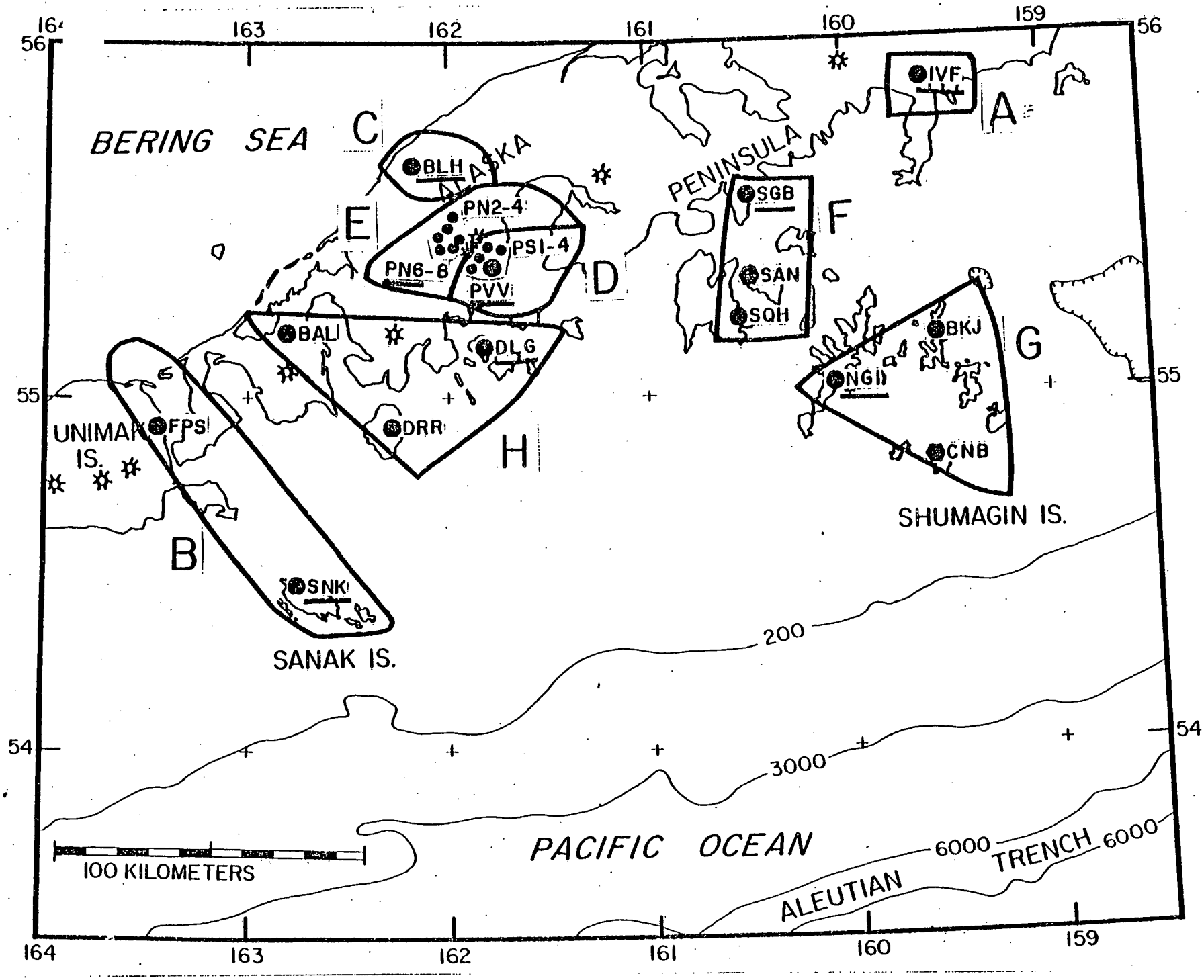

Figure 28b. Map showing the station groupings referred to in part (a). Within each group the signal from the underlined station is input to the signal-detector for that group.

are used: one in a continuous-loop mode to provide a twenty second pre-event "memory", and the other in a standard, reel-to-reel mode to record the data. Frequency-modulated tones from the remote and local sensors are mixed onto the four channels along with an IRIG time code and a frequency-compensation tone (see Figure 29). Eight to ten signals can be mixed onto three of the channels and five can be mixed with the 1000 Hz time code, so that a total of about 32 signals can be recorded. In addition to the tones from the seismic stations, 400 Hz tones from the SMA trigger units are also recorded. Whenever one of these tones is detected the tape recorder is always turned on, so that the on- and off-times of the SMA's can be determined. The magnetic tapes are demodulated, digitized and processed at L-DGO (see discussion under Playback below).

Uninterruptible power-supply (UPS) systems will be installed at DUT and SAN. The battery-back-up portion of the system will be installed in December 1980 and the propane powered alternator units will be installed in the spring or summer of 1981. The battery-backup is designed to provide 4 to 8 hours of uninterrupted power for the entire station should the town power system fail. The propane powered alterntor units are designed to automatically start after about 80% of the battery capacity has been used and to run for about one week without refueling.

The Dutch Harbor recording station and vault were relocated from the old site adjacent to the airport to a concrete bunker on Standard Oil Hill. The old site suffered from proximity to a powerful radio transmitter and the prospect that it would be demolished because it is too close to the landing strip. We have negotiated a reasonable annual lease with the native corporation for use of the new building and power. This summer's field party at Dutch Harbor spent about two weeks refurbishing (insulating, wiring, etc.) the bunker and relocating the equipment there.

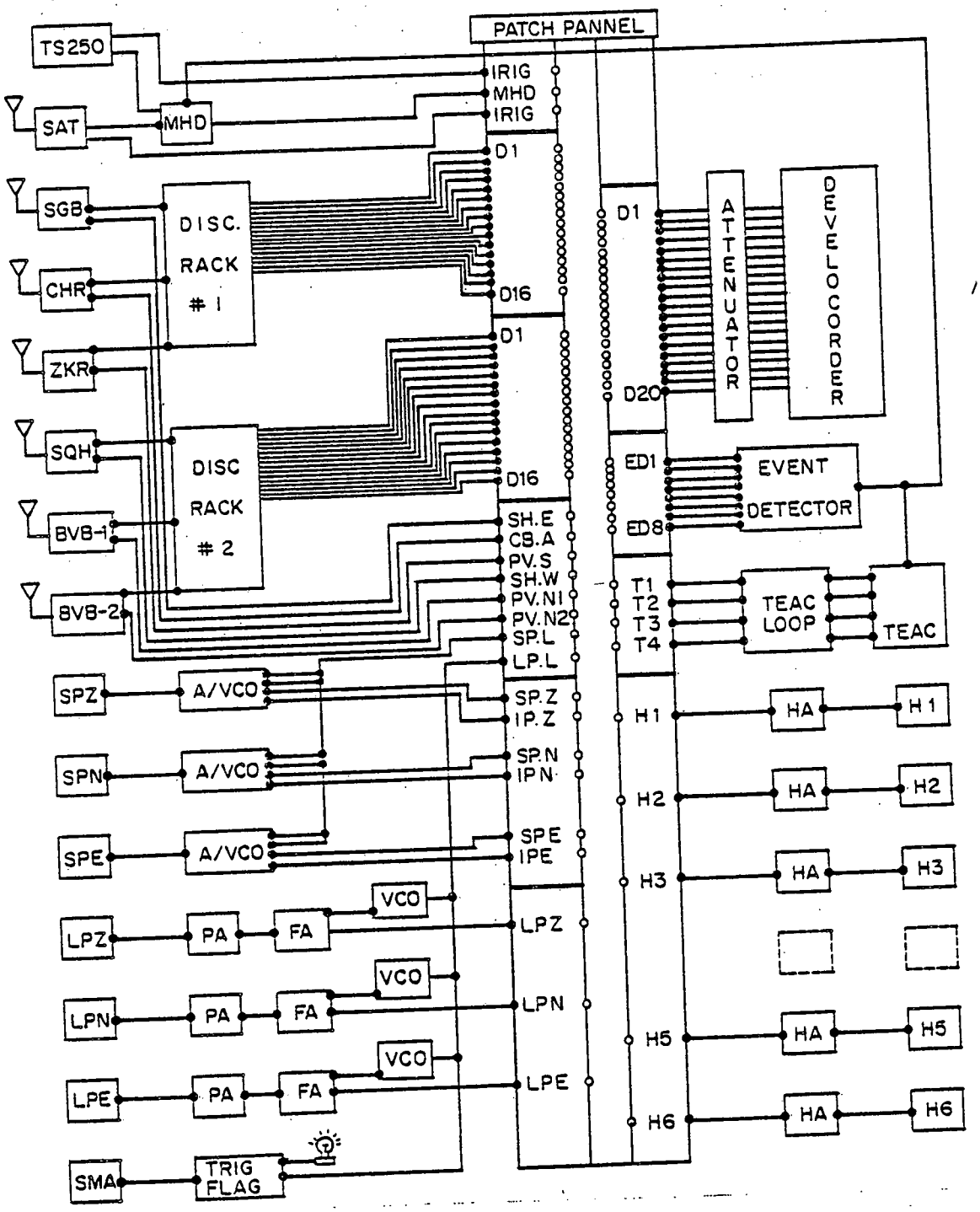

Figure 29. Block diagram for the Sand Point recording center, September 1980. Signal sources are arrayed down the far left of the diagram, signal conditioners are in the middle left, the patch panel in the center, and the recording devices on the right. Signal sources: Sprengnether TS250 chronometer; Kinemetrics satellite receiver for CUT; VHF receivers for subnetworks of the remote seismic stations - SGB (Shumagin-east subnet, SH.E), CHR (Cold Bay subnet, CB.A), ZKR (Pavlof-south subnet, PV.S), SQH (Shumagin-west subnet, SH.W), BVB-1 (Pavlof-north-1 subnet, PV.N1) and BVB-2 (Pavlof-north-2 subnet, PV.N2); SPZ, N and E, the local Baby Benioff, short-period seismometers; LPZ the local Sprengnether long-period vertical seismometer; LPN and E, the local Geotech long-period, horizontal seismometers; and Kinemetrics SMA-1 (1G) strong-motion accelerograph. Signal conditioners: L-DGO min.-hr.-day (MHD) board; discriminator racks 1 and 2; L-DGO two-channel amplifier-VCO units (A-VCO); L-DGO pre- and filter amplifiers (PA and FA) and modified Emtel 6202 VCO, for the long-period signals; and the L-DGO trigger-flag board. All of the signals are available on the patch panel where they can be routed to the event-detector and/or any recording device: Develocorder (18 data channels plus two for time); TEAC tape recorder (four channels, 32 seismic tones plus IRIG time code and tape-speed compensations tones); 5 Helicorders (one channel each, HA = Helicorder amplifier). Note that only the multiplexed output (SH.E through LP.L) are input to the TEAC system and that this system only records when the event-detector declares an event (see Figure 28).

3. Switch to a New Data Analysis System

The L-DGO version of the USGS-PDP 11/70 seismic data analysis system is about 75 percent operational. The hardware and most of the software is now installed. We expect delivery of the software to establish a data base management system to handle the large libraries of digital seismograms that will be created once the new analysis sytem is in routine operation. We can now digitize the demodulated output from the TEAC tape recorders and "pick" the arrival times on a digital seismogram displayed on a fast graphics terminal; the arrival times can then automatically become input to a hypocenter location program and the resultant epicenter be plotted on a map. Even more important than the improved speed and convenience that this system offers is the potential for far more sophisticated waveform analysis. It will be possible, for example, to write programs to analyze converted phases by examining the particle motion recorded by three-component stations, or to make routine estimates of the stress-drop from the shape of the first cycle of the P-wave.

Another advantage of digitizing the seismograms from magnetic tape (or better, digitizing the seismic output) is that during large events, large excursions on the recorder don't overlap onto adjacent channels obscuring information that may otherwise have been available. An example of the sort of improvement that is possible is shown in Figure 30 (a and b).

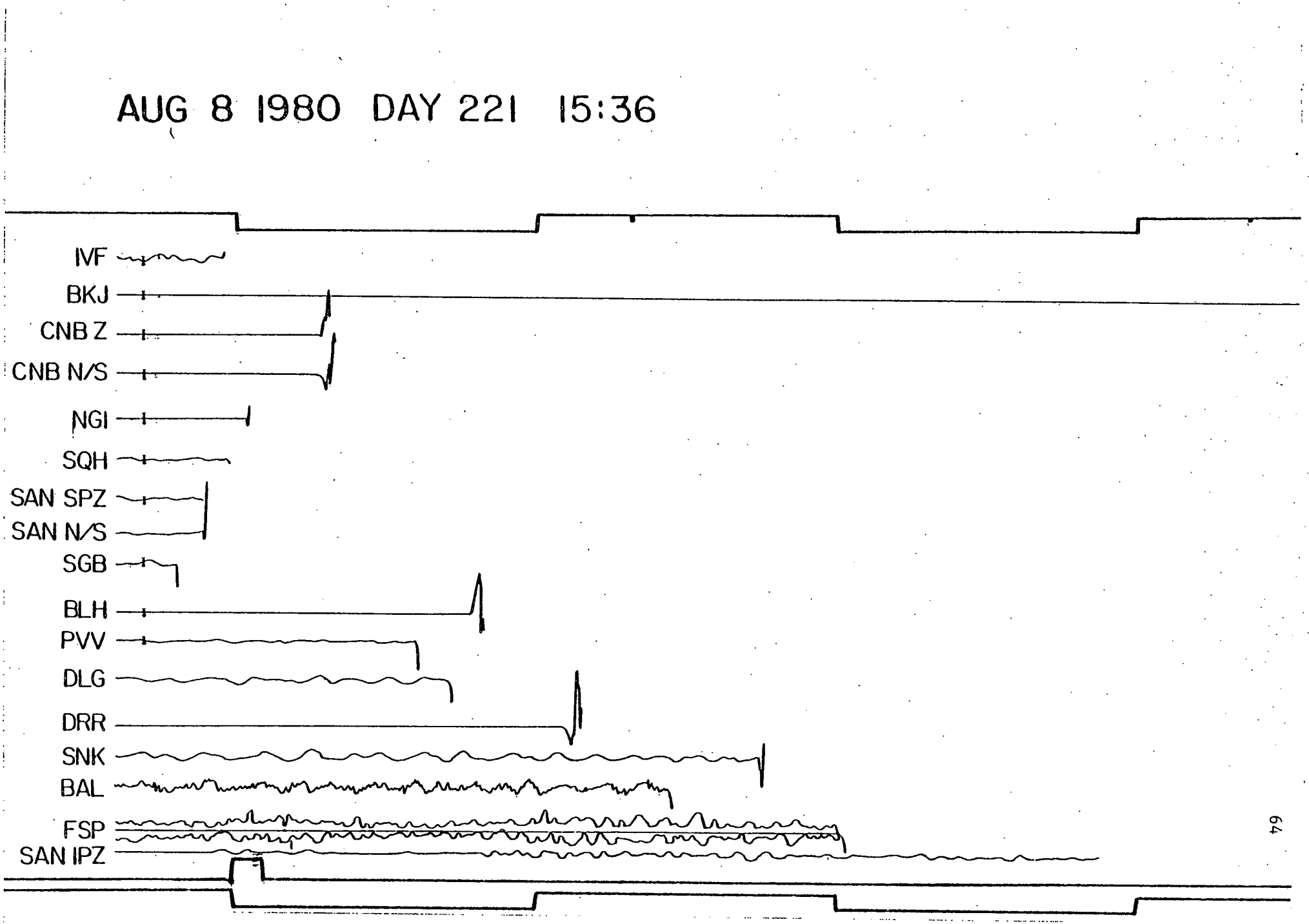

Figure 30a. Sample Develocorder record from 15:36 day 221, 1980. Tracings show the total amount of usable information from this event: the waveforms beyond the first few cycles of the P-wave are either clipped or obscured by the adjacent traces.

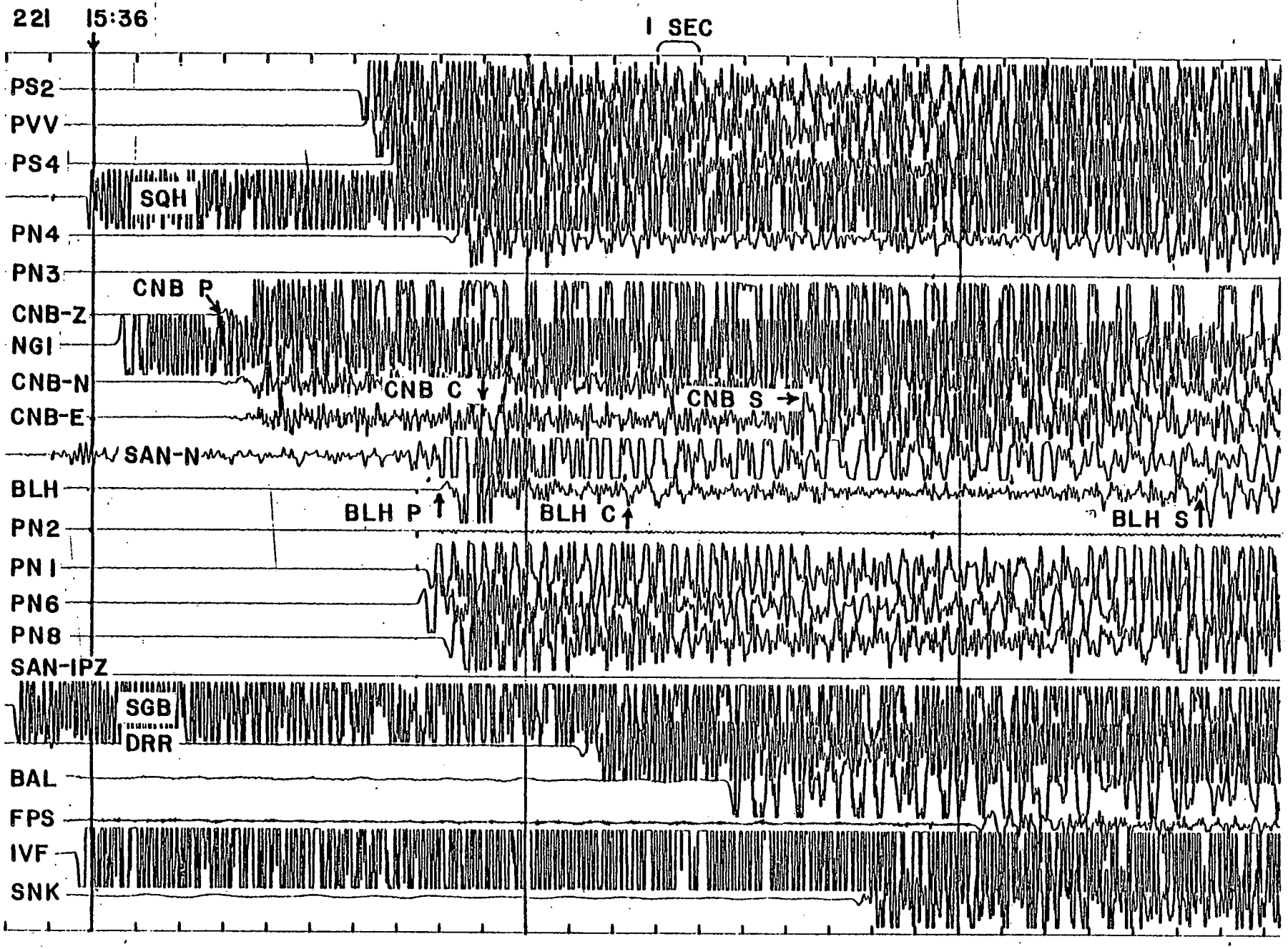

Figure 30b. Sample Versatec record from 15:36 day 221, 1980. This record was created by digitizing the demodulated TEAC tape and then plotting the digital data on a versatec plotter using the PDP 11/70. Note that many of the traces are unclipped and the whole waveform is available for analysis: for examples, note that the signals from CNG and BLH show clear P-, S- and converted (C) phases; these are labelled CNB P, CNB S, CNB C, BLH P, BLH S, and BLH C, respectively.

REFERENCES

Abe, K., 1979. Size of great earthquakes of 1837-1974 inferred from tsunami data, J. Geophys. Res., 84, 1561-1568.

Anderson, D.L., and R.S. Hart, 1978. Q of the Earth, J. Geophys. Res., 83, 5369-5882.

Carpenter, E.W., 1966. Absorption of elastic waves - An operator for constant Q mechanisms, United Kingdom Atomic Energy Authority, Report D-43/66.

Chase, C.G., 1978. Plate kinematics: The Americas, East Africa, and the rest of the world, Earth Planet. Sci. Lett., 37, 355-368, 1978.

Davies, J., L. Sykes, L. House, and K. Jacob, 1981. Shumagin seismic gap, Alaska Peninsula: History of great earthquakes, tectonic setting, and evidence for high seismic potential, in press, J. Geophys. Res..

Der, Z.A., and T.W. McElfresh, 1975. Attenuation of short period P and S waves in the United States, Geophys. J., 40, 85-106.

Eggers, A.A., and D. Chavez, 1979. Temporal gravity variations at Pacaya Volcano, Guatemala, J. Volc. Geotherm. Res., 6, 391-402.

Engdahl, E.R., and C.H. Scholz, 1977. A double Benioff zone beneath the central Aleutians: An unbending of the lithosphere, Geophys. Res. Lett., 4(10), 473-476.

Fukao, Y., 1979. Tsunami earthquakes and subduction processes near deep-sea trenches, J. Geophys. Res., 84, 2303-2314.

Green, C.K., 1946. Seismic sea wave of April 1, 1946, as recorded on tide gauges, Trans. Amer. Geophys. Union, 27, 490-500.

Hanks, T.C., and D.A. Johnson, 1976. Geophysical assessment of peak accelerations, Bull. Seismol. Soc. Amer., 66, 959-968.

Hasegawa, A., N. Umino, and A. Takagi, 1978a. Double-planed structure of the deep seismic zone in the Northeastern Japan arc, Tectonophysics, 47, 43-58.

Hasegawa, A., N. Umino, and A. Takagi, 1978b. Double-planed deep seismic zone and upper mantle structure in the northeastern Japan arc, Geophys. J. R. astr. Soc., 54, 281-296.

Hatori, T., 1969. Dimensions and geographical distribution of tsunami sources near Japan, Bull. Earthq. Res. Inst., Univ. of Tokyo, 47, 185-214.

House, L., L.R. Sykes, J.N. Davies, and K.H. Jacob, 1981. Identification of a possible seismic gap near Unalaska Island, Eastern Aleutians, Alaska, submitted for publication in Maurice Ewing Symposium - Earthquake Prediction, vol. 4, edited by P.G. Richards and D.W. Simpson, to be published by AGU, Washington, D.C.

Iyer, H.M., 1979. Deep structure under Yellowstone National Park, U.S.A.: A continental "hot spot", Tectonophysics, 56, 165-197.

Kanamori, H., 1972a. Tectonic implications of the 1944 Tonankai and the 1946 Nankaido earthquakes, Phys. Earth Planet. Int., 5, 129-139.

Kanamori, H., 1972b. Mechanism of tsunami earthquakes, Phys. Earth Planet. Int., 6, 346-359.

Kanamori, H., 1977. The energy release in great earthquakes, J. Geophys. Res., 82(20), 2981-2988.

Kanamori, H., and K. Abe, 1979. Reevaluation of the turn-of-the-century seismicity peak, J. Geophys. Res., 84(B11), 6131-6139.

Kanamori, H., and G.S. Stewart, 1979. A slow earthquake, Phys. Earth Planet. Int., 18, 167-175.

Kelleher, J., 1972. Rupture zones of large South American earthquakes and some predictions, J. Geophys. Res., 77(11), 2087-2103.

King, P.B., 1967. Tectonic Map of North America, scale 1:5,000,000 (U.S. Geological Survey).

Kondorskaya, N.V., and N.V. Shebalin (editors), 1977. New Catalog of Strong Earthquakes in the Territory of the U.S.S.R., Nauka, Moscow, USSR, 347-433.

Matumoto, T., and R. Page, 1968. Microaftershocks following the Alaskan earthquake of March 28, 1964: Determination of hypocenters and crustal velocities in the Kenai Peninsula-Prince Willian Sound area, Bull. Seismol. Soc. Amer., 58(4), 1131.

McCann, W.R., O.J. Perez, and L.R. Sykes, 1980. Yakataga seismic gap, southern Alaska: Seismic history and earthquake potential, Science, 207, 1309-1314.

McCann, W.R., S.P. Nishenko, L.R. Sykes, and J. Krause, Seismic gaps and plate tectonics: seismic potential for major plate boundaries, Pure Appl. Geophys., 117, 1082-1147.

McNutt, S., 1979. Volcanic earthquakes correlated with earth tides at Pavlof Volcano (abstract), presented at the 1979 NW Section Meeting of the Amer. Geophys. Union, Oregon.

Minster, J.B., and T.H. Jordan, 1978. Present-dat plate motions, J. Geophys. Res., 83, 5331-5354.

Nishenko, S., and W. McCann, 1979. Large thrust earthquakes and tsunamis: Implications for the development of forearc basins, J. Geophys. Res., 84, 573-584.

Perez, O.J., and K.H. Jacob, 1980a. Tectonic model and seismic potential of the eastern Gulf of Alaska and Yakataga seismic gap, J. Geophys. Res., in press.

Perez, O.J., and K.H. Jacob, 1980b. St. Elias, Alaska earthquake of February 28, 1979: Tectonic setting and precursory seismic pattern, Bull. Seismol. Soc. Amer., in press.

Reyners, M., 1980. A microearthquake study of the plate boundary, North Island, New Zealand, Geophys. J. R. astr. Soc., in press.

Reyners, M., and K. Coles, 1981. Fine structure of the dipping seismic zone in the Shumagin Islands, Alaska, in preparation.

Richter, C.F., 1958. Elementary Seismology, W.H. Freeman and Company, San Francisco, California, 768 p.

Shepard, F.P., G.A. Macdonald, and D.C. Cox, 1950. The tsunami of April 1, 1946, Bull. Scripps Inst. Ocean., 5, 391-528.

Sleep, N.H., 1979. The double seismic zone in downgoing slabs and the viscosity of the mesosphere, J. Geophys. Res., 84, 4565-4571.

Solov'iev, S.L., 1968. Sanak-Kodiak Tsunami 1788, Problema Tsunami, Nauka, Moscow, 232-237.

Sommerville, P.G., R.A. Wiggins, and R.M. Ellis, 1976. Time domain determination of earthquake fault parameters from short period P waves, Bull. Seismol. Soc. Amer., 66, 1459-1484.

Sykes, L.R., 1971. Aftershock zones of great earthquakes, seismicity gaps, earthquake prediction for Alaska and the Aleutians, J. Geophys. Res., 76(36), 8021-8041.

Sykes, L.R., J.B. Kisslinger, L. House, J.N. Davies, and K.H. Jacob, 1980. Rupture zones of great earthquakes, Alaska-Aleutian arc, 1784-19[illegible], Science, in press.

Sykes, L.R., J.B. Kisslinger, L. House, J.N Davies, and K.H. Jacob, 19[illegible] Rupture zones and repeat times of great earthquakes along the Alaska-Aleutian arc, 1784-1980, submitted for publication in Ma[illegible]

Symposium - Earthquake Prediction, vol. 4, edited by P.G. Richards and D.W. Simpson, to be published by AGU, Washington, D.C.

Sykes, L.R., and R.C. Quittmeyer, 1981. Repeat times of great earthquakes along simple plate boundaries, submitted for publication in Maurice Ewing Symposium - Earthquake Prediction, vol. 4, edited by P.G. Richards and D.W. Simpson, to be published by AGU, Washington, D.C.

Veith, K.F., 1974. The relationship of island arc seismicity to plate tectonics (abstract), Trans. Amer. Geophys. Union, 55, 349.

3 Reprints Removed

APPENDIX I: Publications

Papers Published or In Press

(1) McCann, W.R., O.J. Perez, and L.R. Sykes, Yakataga seismic gap, southern Alaska: Seismic history and earthquake potential, Science, 207, 1309-1314.

(2) Perez, O.J., and K.H. Jacob, Tectonic model and seismic potential of the eastern Gulf of Alaska and Yakataga seismic gap, J. Geophys. Res., in press, 1980a.

(3) Perez, O.J., and K.H. Jacob, St. Elias, Alaska earthquake of February 28, 1979: Tectonic setting and precursory seismic pattern, Bull. Seismol. Soc. Amer., in press, 1980b.

(4) Davies, J.N., L.R. Sykes, L. House, and K.H. Jacob, Shumagin seismic gap, Alaska Peninsula: History of great earthquakes, tectonic setting, and evidence for high seismic potential, J. Geophys. Res., in press, 1981.

(5) Sykes, L.R., J.B. Kisslinger, L. House, J.N. Davies, and K.H. Jacob, Rupture zones of great earthquakes, Alaska-Aleutian arc, 1784-1980, Science, in press, 1980.

(6) Boatwright, J., Preliminary body wave analysis of the St. Elias, Alaska earthquake of February 28, 1979, Bull. Seismol. Soc. Amer., 70, 419-436, 1980.